Robust T cell activation requires an eIF3-driven burst in T cell receptor translation

Authors: Dasmanthie De Silva[1,2], Lucas Ferguson[1], Grant H. Chin[1], Benjamin E. Smith[3], Ryan A. Apathy[4], Theodore L. Roth[4], Franziska Blaeschke[5], Marek Kudla[1], Alexander Marson[4,5,6,7,8,9,10], Nicholas T. Ingolia[1,11], Jamie H. D. Cate[1,2,10,11,12,13]*.

Affiliations:

[1]Department of Molecular and Cell Biology, University of California-Berkeley, Berkeley, California 94720, USA.

[2]The J. David Gladstone Institutes, San Francisco, CA 94158 USA.

[3]School of Optometry, University of California, Berkeley, Berkeley, CA 94720, USA.

[4]Department of Microbiology and Immunology, University of California, San Francisco, San Francisco, CA, USA.

[5]Gladstone-UCSF Institute of Genomic Immunology, San Francisco, CA 94158 USA.

[6]Diabetes Center, University of California, San Francisco, San Francisco, CA, USA.

[7]Chan Zuckerberg Biohub, San Francisco, CA, USA.

[8]Department of Medicine, University of California, San Francisco, San Francisco, CA, USA.

[9]Parker Institute for Cancer Immunotherapy, San Francisco, CA, USA.

[10]Innovative Genomics Institute, University of California, Berkeley, Berkeley, CA, USA.

[11]California Institute for Quantitative Biosciences, University of California, Berkeley, Berkeley, USA.

[12]Department of Chemistry, University of California-Berkeley, Berkeley, California 94720, USA.

[13]Molecular Biophysics and Integrated Bioimaging Division, Lawrence Berkeley National Laboratory, Berkeley, California 94720, USA.

*Correspondence to: j-h-doudna-cate@berkeley.edu.

ABSTRACT

Activation of T cells requires a rapid surge in cellular protein synthesis. However, the role of translation initiation in the early induction of specific genes remains unclear. Here we show human translation initiation factor eIF3 interacts with select immune system related mRNAs including those encoding the T cell receptor (TCR) subunits TCRA and TCRB. Binding of eIF3 to the *TCRA* and *TCRB* mRNA 3'-untranslated regions (3'-UTRs) depends on CD28 coreceptor signaling and regulates a burst in TCR translation required for robust T cell activation. Use of the *TCRA* or *TCRB* 3'-UTRs to control expression of an anti-CD19 chimeric antigen receptor (CAR) improves the ability of CAR-T cells to kill tumor cells *in vitro*. These results identify a new mechanism of eIF3-mediated translation control that can aid T cell engineering for immunotherapy applications.

KEYWORDS

eIF3, protein synthesis, 3'-untranslated region, T cell receptor, CD28, chimeric antigen receptor, cellular immunotherapy

INTRODUCTION

Translation initiation serves as a key gatekeeper of protein synthesis in eukaryotes and requires the action of eukaryotic initiation factor 3 (eIF3) (Hernández et al., 2020; Pelletier and Sonenberg, 2019). In humans, eIF3 is a 13-subunit protein complex that coordinates the cellular machinery in positioning ribosomes at the mRNA start codon. Several lines of evidence indicate eIF3 also serves specialized roles in cellular translation, by recognizing specific RNA structures in the 5'-untranslated regions (5'-UTRs) of target mRNAs (Lee et al., 2015), binding the 7-methyl-guanosine (m^7G) cap (Lamper et al., 2020; Lee et al., 2016) or through interactions with *N*-6-methyl-adenosine (m^6A) post-transcriptional modifications in mRNAs (Meyer et al., 2015). Binding to these *cis*-regulatory elements in mRNA can lead to translation activation or repression, depending on the RNA sequence and structural context (Lee et al., 2016, 2015; Meyer et al., 2015; de la Parra et al., 2018). These noncanonical functions for eIF3 can aid cell proliferation (Lee et al., 2015), or allow cells to rapidly adapt to stresses such as heat shock (Meyer et al., 2015). T cell activation requires a rapid increase in protein synthesis within the first few hours that also involves eIF3 (Ahern et al., 1974; Kleijn and Proud, 2002; Miyamoto et al., 2005; Ricciardi et al., 2018). However, whether eIF3 serves a general or more specific role in T cell activation is unknown.

Translation in non-activated lymphocytes is limited by the availability of translation initiation factors (Ahern et al., 1974; Mao et al., 1992; Wolf et al., 2020). The mRNAs for several translation initiation factors, including those for many eIF3 subunits, are repressed in resting T cells and are rapidly translated within hours of activation (Wolf et al., 2020). Additionally, nearly-inactive eIF3 in quiescent T cells is activated to form translation

initiation complexes in the first few hours after stimulation (Miyamoto et al., 2005). Activation of eIF3 coincides with the recruitment of subunit eIF3j to eIF3 and translation initiation complexes (Miyamoto et al., 2005). Post-translational modifications are also thought to contribute to the early increase in translation, for example activation of the guanine nucleotide exchange factor eIF2B (Kleijn and Proud, 2002). By contrast, the level of the canonical mRNA cap-binding complex eIF4F–composed of translation initiation factors eIF4E, eIF4G and eIF4A– increases much later after T cell activation (Mao et al., 1992).

Recent studies have identified translational control of specific transcripts required for the rewiring of metabolism needed for effector T cell function. Translation of these specific transcripts involved in glycolysis and fatty acid synthesis occurs within 1-3 days of T cell activation (Ricciardi et al., 2018), and depends on the activity of eIF4F. Hundreds of other mRNAs translationally repressed in resting T cells are rapidly translated within hours after activation, including those encoding key transcription factors and ribosomal proteins, in addition to the translation initiation factors noted above (Wolf et al., 2020). Most of these mRNAs are sensitive to mTOR inhibition, highlighting the importance of eIF4F for the translation of these specific transcripts. However, a small subset of mRNAs evade mTOR inhibition by an unknown mechanism (Wolf et al., 2020). Whether eIF3 selectively regulates these or other mRNAs early in T cell activation is not known.

In the adaptive immune system, T cells are activated when a foreign antigen is recognized by the T cell receptor (TCR). However, robust T cell activation requires a second signal generated by interactions between the T cell and antigen presenting cell mediated by the co-receptor CD28 (Esensten et al., 2016). This two-signal mechanism

enables T cells to adopt a fully active state and avoid becoming unresponsive (Chen and Flies, 2013). The process of T cell activation can be mimicked *in vitro* using antibodies targeting both the TCR and CD28 (anti-CD3 and anti-CD28 antibodies, respectively) (Harding et al., 1992), which has greatly aided the dissection of molecular mechanisms underlying T cell activation.

Insights from these studies have also inspired efforts to engineer T cells for immunotherapy applications such as treating cancers (Chen and Flies, 2013). T cells can be engineered to express chimeric antigen receptors (CARs) that specifically target antigens on the surface of cancer cells, and signal through protein elements derived from both the TCR and CD28 or other co-stimulatory receptors (Chen and Flies, 2013; Globerson Levin et al., 2021). The most successful of these CAR T cells have been used to treat CD19-positive B cell malignancies, with dramatic results (Friedman et al., 2018; Kalos et al., 2011; Kochenderfer et al., 2013; Qin et al., 2020; Wang et al., 2020). However, CAR T cells still have a number of drawbacks, including toxicity, CAR T cell exhaustion, limited persistence and poor efficacy in solid tumors. These problems highlight the need for a deeper understanding of T cell activation and how it can be controlled in CAR T cells (Globerson Levin et al., 2021; Watanabe et al., 2018).

Here, we identified mRNAs that specifically bind eIF3 in activated T cells, including many encoding proteins involved in immune cell function such as the TCR. We mapped the eIF3-dependent *cis*-regulatory elements in the mRNAs encoding the TCR alpha and beta subunits (TCRA and TCRB, respectively), finding the 3'-untranslated regions (3'-UTRs) of these mRNAs control a rapid burst in TCRA and TCRB translation that depends on CD28 coreceptor signaling. Finally, we use this information to engineer T cells

expressing chimeric antigen receptors to modulate the dynamics of CAR expression and improve the ability of CAR T cells to kill tumor cells *in vitro*.

RESULTS

A specific suite of RNAs interact with eIF3 in activated Jurkat cells

To delineate how eIF3 contributes to T cell activation, we first identified RNAs that directly interact with eIF3 in Jurkat cells activated for 5 hours with phorbol 12-myristate 13-acetate and ionomycin (PMA+I), using photoactivatable ribonucleoside-enhanced crosslinking and immunoprecipitation (PAR-CLIP) (Hafner et al., 2010; Lee et al., 2015; Mukherjee et al., 2019) (**Figure 1A**). In the Jurkat PAR-CLIP experiments, RNA crosslinked to eight of the thirteen eIF3 subunits, as identified by mass spectrometry: subunits EIF3A, EIF3B, EIF3D and EIF3G as previously seen in HEK293T cells (Lee et al., 2015), as well as subunits EIF3C, EIF3E, EIF3F, and EIF3L (**Figure 1B, Figure 1–figure supplement 1A-1B, Supplementary File 1**). Consistent with its role in T cell activation, eIF3 crosslinked to a substantially larger number of mRNAs (~75x more) in activated Jurkat cells compared to control non-activated cells (**Figure1–figure supplement 1C-1D and Supplementary Files 2 and 3**). Notably, in activated Jurkat cells eIF3 interacted with mRNAs enriched for those encoding proteins central to immune cell function, in contrast to those previously identified in HEK293T cells (Lee et al., 2015) (**Figure 1C and Figure 1–figure supplement 1E**). The extent of eIF3 crosslinking in activated Jurkat cells does not correlate with mRNA abundance (**Figure 1–figure supplement 1F and Supplementary File 4**), suggesting the enrichment of immune

system related mRNAs reflects the involvement of eIF3 in specific regulation of T cell activation.

In activated Jurkat cells, eIF3 showed a multitude of crosslinking patterns on different mRNAs (**Figure 1D-1E and Figure 1–figure supplement 1D, 1G and 1H**), consistent with varied roles for eIF3 in T cell activation and function. Many of the mRNAs have a single PAR-CLIP site in the 5'-UTR as observed in HEK293T cells (Lee et al., 2015) (**Figure 1D, Figure 1–figure supplement 1D, Supplementary File 3**). However, eIF3 crosslinked to some mRNAs across the entire length of the transcript, from the beginning of the 5'-UTR through the 3'-UTR (**Figure 1E and Figure 1–figure supplement 1H**). This "pan-mRNA" pattern of eIF3 crosslinking–which includes polyadenylated mRNAs as well as histone mRNAs–has not been observed before. Interestingly, a number of these mRNAs encode proteins important for T cell activation, including both the alpha and beta subunits of the T cell receptor (TCR), subunits TCRA and TCRB (**Figure 1E, Supplementary File 5**).

TCRA and *TCRB* mRNAs form distinct puncta in activated Jurkat cells

Crosslinking in PAR-CLIP experiments requires direct interaction between the RNA and protein of interest (Ascano et al., 2012). Thus, the pan-mRNA pattern of crosslinking between eIF3 and certain mRNAs suggests formation of ribonucleoprotein complexes (RNPs) highly enriched in eIF3. Notably, the pan-mRNA crosslinking pattern in the *TCRA* and *TCRB* mRNAs occurs in activated but not in non-activated Jurkat cells (**Figure 1E**), suggesting eIF3 may contribute to increased translation of these mRNAs rather than their repression. We therefore examined *TCRA* and *TCRB* mRNA localization

in activated Jurkat cells, to determine whether they colocalized with repressive environments such as P bodies or stress granules (Tauber et al., 2020). Since Jurkat cells have a defined TCR, we designed fluorescence in situ hybridization (FISH) probes across the entire *TCRA* and *TCRB* transcripts to examine their localization. Interestingly, the *TCRA* and *TCRB* mRNAs formed distinct puncta in Jurkat cells activated with anti-CD3/anti-CD28 antibodies, which induce both TCR and CD28 coreceptor signaling required for robust T cell activation (Harding et al., 1992). However, these mRNAs did not co-localize with either P bodies or stress granules, or with each other (**Figure 1F, Figure 1–figure supplement 2A and 2B**). These results indicate that the *TCRA* and *TCRB* mRNAs are not translationally repressed but are likely localized to translation "hot spots."

Pan-mRNAs remain bound to eIF3 in translating ribosomes

The pan-mRNA crosslinking pattern suggests that eIF3 remains bound to the *TCRA* and *TCRB* mRNAs while they are actively translated. To capture *TCRA* and *TCRB* mRNAs in translating ribosomes and examine their interactions with eIF3, we analyzed polysomes in Jurkat cells activated with anti-CD3/anti-CD28 antibodies (**Figure 2A**) (Harding et al., 1992). The cells were first treated with protein-protein crosslinker dithiobis(succinimidyl propionate) (DSP) before isolating polysomes on sucrose gradients (**Figure 2–figure supplement 1A**). We then incubated the cell lysates with RNase H and DNA oligonucleotides designed to cleave the mRNAs specifically between the 5'-UTR, coding sequence (CDS), and 3'-UTR (**Figure 2B, Supplementary File 6**). This protocol efficiently cleaved the mRNAs and prevented the released 5'-UTR and 3'-UTR elements from entering polysomes (**Figure2–figure supplement 1B-1E**). It also allowed us to

detect eIF3 interactions with the mRNA CDS regions independent of eIF3 interactions with the UTR sequences identified in the PAR-CLIP analysis. We detected mRNAs interacting with eIF3 in the polysomes by performing anti-EIF3B immunoprecipitations followed by qRT-PCR (**Figure 2A**). We compared both *TCRA* and *TCRB* mRNAs to another pan-crosslinked mRNA, *DUSP2*, and to two mRNAs that crosslinked to eIF3 only through their 5'-UTRs (*EGR1*, *TRIM28*). Using primers to the CDS regions of the mRNAs, we found that eIF3 only immunoprecipitated the pan-crosslinked mRNAs (*TCRA*, *TCRB*, *DUSP2*) from polysomes, but not mRNAs that only crosslinked to eIF3 through their 5'-UTRs (*EGR1*, *TRIM28*) (**Figure 2C and 2D**). Importantly, all of these mRNAs are present in translating ribosomes and can be immunoprecipitated with eIF3 when the mRNAs are left intact (RNase H treatment without DNA oligos) (**Figure 2E**).

We also tested whether these mRNAs interact with eIF3 similarly in primary human T cells during activation. We could not examine *TCRA* and *TCRB* mRNAs in primary human T cells, as these mRNAs do not have a unique sequence in the 5'-UTR or variable region of the CDS to which we could design DNA oligonucleotides as described above. Therefore, we tested the distribution of *DUSP2*, *EGR1* and *TRIM28* mRNAs in primary human T cells activated with anti-CD3/anti-CD28 antibodies (Harding et al., 1992). As observed in Jurkat cells, *DUSP2* mRNA remained bound to eIF3 through its CDS region in polysomes whereas the *EGR1* and *TRIM28* mRNAs did not remain bound (**Figure 2F–2H**). We also confirmed that the 5'-UTR and 3'-UTR elements of these mRNAs are efficiently cleaved and did not enter polysomes (**Figure2–figure supplement 1F–1H**). Taken together, these results indicate that, in activated T cells, eIF3 remains bound to the coding sequences (CDS) of the pan-mRNAs *TCRA*, *TCRB* and *DUSP2* in polysomes

independent of their 5'-UTR and 3'-UTR elements. These results further support the model that *TCRA* and *TCRB* mRNA puncta represent translation "hot spots," and the pan-mRNA crosslinking pattern reflects eIF3 binding to these mRNAs during translation elongation.

eIF3 interacts with the *TCRA* and *TCRB* mRNA 3'-UTRs and controls a burst in translation during T cell activation

Although crosslinking of eIF3 to the CDS regions of the *TCRA* and *TCRB* mRNAs (**Figure 1E**) indicates eIF3 remains bound to them during translation elongation (**Figure 2 and Figure 2–figure supplement 1**), we wondered whether the 5'-UTRs and 3'-UTRs might play a role in recruiting these mRNAs to translating ribosomes. The *TCRA* and *TCRB* genes encode a different, often short 5'-UTR for each variable region of the mature locus (Omer et al., 2021; Scaviner and Lefranc, 2000), suggesting the 5'-UTR is unlikely to harbor eIF3-dependent regulatory elements. We therefore focused on the roles of the *TCRA* and *TCRB* 3'-UTRs. We constructed nanoluciferase reporters fused to the WT *TCRA* or *TCRB* mRNA 3'-UTR sequence, to 3'-UTRs with the eIF3 PAR-CLIP site deleted (*ΔPAR*) or to 3'-UTRs with the reversed sequence of the eIF3 PAR-CLIP site (R**PAR*, i.e. 5'-3' sequence reversed to 3'-5' direction to maintain the length of the 3'-UTR) (**Figure 3A**). We then stably expressed these mRNAs in primary human T cells using lentiviral transduction and activated these T cells using anti-CD3/anti-CD28 antibodies. T cells expressing the reporters with the WT *TCRA* or *TCRB* mRNA 3'-UTR sequences produced substantially higher luminescence that peaked 1 hour after activation, while cells expressing nanoluciferase from reporters with a deletion or reversal of the eIF3 PAR-

CLIP site sequence showed no apparent burst in translation (**Figure 3B**). The *TCRA* Δ*PAR* or R**PAR* or *TCRB* Δ*PAR* or R**PAR* mutations, however, did not cause significant defects in the nanoluciferase mRNA levels when compared to reporters with the corresponding WT 3'-UTR sequences (**Figure 3C**)**.** This suggests the burst in nanoluciferase expression observed with the WT *TCRA* or *TCRB* mRNA 3'-UTR sequences is regulated posttranscriptionally. Immunoprecipitation of eIF3 followed by qRT-PCR quantification of nanoluciferase mRNA showed that less nanoluciferase mRNA bound to eIF3 when the 3'-UTR PAR-CLIP site was either deleted or reversed, compared to nanoluciferase mRNAs carrying the WT *TCRA* or *TCRB* 3'-UTR (**Figure 3D and 3E**). Interestingly, although the *TCRA* and *TCRB* mRNA 3'-UTR elements that crosslinked to eIF3 do not share any conserved sequences or RNA structural elements (Xu and Mathews, 2016), the above results support the idea that eIF3 binding to specific sequences or structures within the *TCRA* and *TCRB* 3'-UTRs controls a burst in translation after T cell activation.

We next tested whether the *TCRA* and *TCRB* 3'-UTRs serve to initially recruit eIF3 to the *TCRA* and *TCRB* mRNAs, as eIF3 does not remain stably bound to these 3'-UTRs in translating ribosomes (**Figure 1–figure supplement 2G**). We made nanoluciferase reporters in which we replaced the eIF3 PAR-CLIP site in the *TCRA* 3'-UTR with sequences from the hepatitis C viral internal ribosome entry site (HCV IRES domain IIIabc) or the *JUN* mRNA 5'-UTR, each previously shown to bind directly to eIF3 (Kieft et al., 2001; Lee et al., 2015) (**Figure 3F**). We stably transduced these constructs into primary T cells and measured nanoluciferase activity after activating the cells with anti-CD3/anti-CD28 antibodies. By contrast to the *TCRA* Δ*PAR* 3'-UTR, the HCV IRES IIIabc

and *JUN* sequences increased nanoluciferase translation (**Figure 3G**). This was true despite the fact that there was less of an increase in mRNA abundance for the HCV IRES IIIabc and *JUN* constructs compared to the *TCRA* Δ*PAR* 3'-UTR (**Figure 3H**). The HCV IRES IIIabc and *JUN* sequences also rescued eIF3 binding to the reporter mRNAs (**Figure 3I**) upon T cell activation. These results are consistent with the engineered 3'-UTRs recruiting eIF3 to the mRNA. However, the dynamics of translation activation induced by the 3'-UTRs harboring the HCV IRES or *JUN* sequences did not recapitulate the effects of the WT *TCRA* 3'-UTR. Both engineered 3'-UTRs increased nanoluciferase levels within 30 minutes of activation, in contrast to the WT *TCRA* 3'-UTR (**Figure 3G**). Furthermore, neither engineered 3'-UTR led to a marked decrease of nanoluciferase levels after the 1 hour peak in luminescence seen with the WT *TCRA* 3'-UTR (**Figure 3G**). Taken together, the nanoluciferase reporter experiments reveal the *TCRA* and *TCRB* mRNA 3'-UTRs are necessary and sufficient to drive a burst in translation after T cell activation. They also suggest these 3'-UTR elements recruit eIF3 to the *TCRA* and *TCRB* mRNAs to drive a burst in translation of the TCR alpha and beta subunits.

The *TCRA* and *TCRB* mRNA 3'-UTRs control a burst in translation in a CD28-dependent manner

Since T cell activation in some cases does not require the TCR (Siefken et al., 1998), we also tested whether the burst in translation controlled by the *TCRA* and *TCRB* mRNA 3'-UTRs could be induced by activation of either the TCR or CD28 individually (**Figure 4**). We found anti-CD28 stimulation alone was sufficient to cause a transient burst in translation in the nanoluciferase reporters with the WT *TCRA* or *TCRB* mRNA 3'-UTRs,

whereas anti-CD3 stimulation caused a continuous increase in reporter protein expression (**Figure 4B–4D**). Interestingly, the burst in translation required the reporters to be membrane tethered via a N-terminal transmembrane helix (from CD3zeta) that is co-translationally inserted into the membrane (Call and Wucherpfennig, 2005) (**Figure 4A–4D and Figure 4–figure supplement 1A–1C**), consistent with the fact that CD28 signaling involves multiple membrane-associated events (Boomer and Green, 2010). Moreover, the reporters with *TCRA* Δ*PAR* and *TCRB* Δ*PAR* 3'-UTRs failed to show a burst in expression even when the reporter proteins were tethered to the membrane (**Figure 4A–4D**), supporting the role for eIF3 in the translational burst. Taken together, these results support the model that the CD28 costimulatory pathway drives an early burst in TCR translation after T cell activation, mediated by eIF3 binding to the *TCRA* and *TCRB* 3'-UTRs.

We also tested the proximal signaling pathways downstream of CD28 required for the dynamic regulation of reporter expression by using inhibitors of the kinases AKT (Choi et al., 2016; Wu et al., 2020) and mTOR (Thoreen et al., 2009). In T cells expressing the membrane-tethered nanoluciferase reporter mRNA with the WT *TCRA* 3'-UTR (**Figure 4A**), treatment with the mTOR inhibitor Torin 1 had no effect on the rapid increase in reporter expression as seen with the DMSO control. However the burst in nanoluciferase expression was blocked when AKT kinase activity was inhibited with AZD5363 (AZD) (**Figure 4E–4F and Figure 4–figure supplement 1D-1E**). Altogether, these data indicate that the transient burst in TCR expression likely requires specific interactions between eIF3 and the *TCRA* and *TCRB* 3'-UTRs and also membrane-proximal CD28 signaling. Furthermore, these results support a model in which T cell activation requires CD28

317 costimulation to elicit an initial positive signal involving AKT kinase activity, which is later
318 repressed by a negative feedback loop also mediated by CD28 signaling and cis-
319 regulatory elements in the *TCRA* and *TCRB* mRNA 3'-UTRs.

320

321 **eIF3 interactions with the *TCRA* and *TCRB* mRNA 3'-UTRs regulate a burst in TCR**
322 **translation important for T cell activation**

323 Given that the *TCRA* and *TCRB* mRNA 3'-UTRs are necessary and sufficient to
324 drive a burst in translation after T cell activation, we examined their effects on the
325 endogenous levels of the TCR. We analyzed the expression of TCR protein levels using
326 western blots probed with an anti-TCRA antibody, since the formation of an intact TCR is
327 required to stabilize both the TCRA and TCRB subunits (Koning et al., 1988; Ohashi et
328 al., 1985). As seen with the nanoluciferase reporters, TCRA levels rose and peaked
329 approximately one hour after T cell activation with anti-CD3/anti-CD28 antibodies (**Figure**
330 **5A**). Furthermore, the early burst in TCRA translation is dependent on CD28 but not on
331 TCR signaling (**Figure 5A**), also as observed with membrane-tethered reporters (**Figure**
332 **4**). To more directly assess the role of the *TCRA* and *TCRB* mRNA 3'-UTRs, we used
333 CRISPR-Cas9 genome editing to delete the eIF3 PAR-CLIP sites in either the *TCRA* or
334 *TCRB* mRNA 3'-UTRs in primary T cells from two healthy human donors (**Figure 5–figure**
335 **supplement 1A and Supplementary File 6**). PCR analysis showed successful deletion
336 of the eIF3 PAR-CLIP site in the *TCRA* 3'-UTR or in the *TCRB* 3'-UTR (*TCRA* Δ*PAR* or
337 *TCRB* Δ*PAR*, respectively) in 43% - 49% of the alleles (**Figure 5–figure supplement**
338 **1B**). A scrambled sgRNA (SC), which does not target any site in the human genome was
339 used as a control. We first measured the total endogenous TCRA protein levels by

western blot in *TCRA* or *TCRB* 3'-UTR edited cells versus control cells at different time points after activating with anti-CD3/anti-CD28 antibodies (**Figure 5B**). The SC control cells – which should behave as wild-type T cells – exhibited a substantial burst in TCRA protein levels immediately after activation (~1 hr). By contrast, TCRA protein levels were nearly absent or clearly reduced at early time points after activation in both *TCRA* Δ*PAR* and *TCRB* Δ*PAR* cell populations (**Figure 5B**). Only at later time points did TCRA levels in the *TCRA* Δ*PAR* and *TCRB* Δ*PAR* cell populations begin to increase. These results share the same pattern of expression seen with the nanoluciferase reporters described above (**Figure 3 and Figure 4**).

We next asked whether the burst in TCR expression driven by the *TCRA* and *TCRB* 3'-UTRs affected downstream steps in T cell activation. During TCR-dependent T cell activation, membrane proteins reorganize at the interface between the T cell and antigen presenting cell (APC) to form an immunological synapse (Huppa and Davis, 2003). TCR cluster formation is a central aspect of immune synapse formation (Cochran et al., 2001). Therefore we tested whether TCR cluster formation is affected by reduced TCR protein levels in *TCRA* Δ*PAR* and *TCRB* Δ*PAR* T cells at early time points after activation. We used the same cell populations as those used for the western blots above (**Figure 5B**), to correlate the TCRA protein levels observed in the western blots with TCR clustering. We performed immunofluorescence on SC, *TCRA ΔPAR* and *TCRB ΔPAR* T cell populations using anti-TCRA and anti-TCRB antibodies to detect the TCR. Both *TCRA* Δ*PAR* and *TCRB* Δ*PAR* cells had fewer cells forming TCR clusters, especially at the early time point compared to SC control cells when activated with anti-CD3/anti-CD28 (**Figure 5C and Figure 5–figure supplement 1C**). Consistent with the TCRA expression

levels observed in western blots and the rate of TCR clustering (**Figure 5B and 5C**), both *TCRA* Δ*PAR* and *TCRB* Δ*PAR* cells expressed lower amounts of cell surface TCR compared to SC control cells or cells edited with a single gRNA when tested by flow cytometric analysis after PMA+I activation (**Figure 5–figure supplement 1D and 1E**).

To test whether the defect in TCR clustering in the *TCRA* Δ*PAR* and *TCRB* Δ*PAR* cell populations reflects a general deficiency in T cell activation, we measured the T cell activation markers CD69 and CD25 (IL2RA) by flow cytometry (**Figure 5–figure supplement 1F and Figure 5–figure supplement 2A and 2B**). Fewer cells in the *TCRA* Δ*PAR* and *TCRB* Δ*PAR* CD8+ and CD4+ primary T cell populations expressed CD69 at early time points after activation (5-8 hours) (**Figure 5–figure supplement 2C and 2D**) and fewer expressed both CD69 and CD25 at later time points after activation, compared to SC control cells (**Figure 5D–5E and Figure 5–figure supplement 2E and 2F**). We also found the *TCRA* Δ*PAR* and *TCRB* Δ*PAR* T cell populations secreted lower amounts of cytokines IL2 (**Figure 5F and Figure 5–figure supplement 2G)** and IFNγ (**Figure 5G and Figure 5–figure supplement 2H**), compared to the SC control cells. Taken together, the *TCRA* Δ*PAR* and *TCRB* Δ*PAR* primary T cell populations exhibited multiple early and late T cell activation defects. These results support the model that after T cell activation, eIF3 binding to the *TCRA* and *TCRB* mRNA 3'-UTRs drives an early burst in TCR translation that is required for many subsequent steps in T cell activation.

To obtain additional mechanistic understanding of eIF3-mediated regulation of TCR translation we generated clonal *TCRA* Δ*PAR* and *TCRB* Δ*PAR* Jurkat cells using the CRISPR-Cas9 genome editing strategy developed for primary T cells (**Figure 5–figure supplement 1A, Supplementary File 6**). We first measured total TCR levels

using western blots and an anti-TCRA antibody as described above (**Figure 5A**), at different time points after activation with anti-CD3/anti-CD28 antibodies. WT Jurkat cells showed a TCR translational burst that peaked 5-8 hours after activation (**Figure 5–figure supplement 3A**). By contrast, both *TCRA* Δ*PAR* and *TCRB* Δ*PAR* Jurkat cell populations expressed lower levels of the TCR proteins compared to WT cells, and failed to show a burst in TCR expression at early time points after activation (**Figure 5–figure supplement 3A**). Importantly, *TCRA* and *TCRB* mRNA levels were unaffected or even increased in the *TCRA* Δ*PAR* and *TCRB* Δ*PAR* Jurkat cells (**Figure 5–figure supplement 3B and 3C**), similar to our observations with nanoluciferase reporters in primary T cells (**Figure 3C**). This is consistent with TCR expression levels being regulated post-transcriptionally by eIF3 interactions with the *TCRA* or *TCRB* mRNA 3'-UTR elements. We then tested whether deleting eIF3 binding sites in both *TCRA* and *TCRB* mRNA 3'-UTRs affected their interaction with eIF3. In both *TCRA* Δ*PAR* and *TCRB* Δ*PAR* cells, eIF3 bound to significantly lower amounts of the *TCRA* and *TCRB* mRNAs compared to WT cells at both the 5 hour and 8 hour time points after anti-CD3/anti-CD28 activation (**Figure 5–figure supplement 3D and 3E**). This indicates deleting the eIF3 PAR-CLIP sites in the 3'-UTR disrupts eIF3 interactions with the *TCRA* and *TCRB* mRNAs substantially. Together with the nanoluciferase reporter experiments in primary T cells (**Figure 3**), these results support the model that eIF3 binding to the 3'-UTR elements of the *TCRA* and *TCRB* mRNAs mediates the rapid burst in TCR translation after T cell activation.

The *TCRA* and *TCRB* mRNA 3'-UTRs enhance anti-CD19 CAR T cell function

T cells engineered to express chimeric antigen receptors (CARs) for cancer immunotherapy now in use clinically employ artificial 3'-UTRs in the CAR-encoding mRNA, a woodchuck hepatitis viral posttranscriptional regulatory element (*WPRE*) (Milone et al., 2009), or a retroviral 3'-long terminal repeat (*3'-LTR*) (Kochenderfer et al., 2009). However, it is not known whether these 3'-UTR elements provide optimal CAR expression or CAR T cell function. To test whether these 3'-UTRs induce a transient burst in translation as observed with the WT *TCRA* or *TCRB* 3'-UTRs, we fused the *WPRE* and *3'-LTR* 3'-UTR sequences to nanoluciferase reporters and expressed these in primary T cells (**Figure 6A**). In contrast to the *TCRA* and *TCRB* 3'-UTRs (**Figure 3 and Figure 4**), the *WPRE* and *3'-LTR* 3'-UTR elements failed to induce the early burst in nanoluciferase expression (**Figure 6A**). These data suggest that fusing the *TCRA* or *TCRB* 3'-UTR sequences to engineered CAR open reading frames could be used to obtain more physiological expression dynamics seen for the endogenous TCR.

We therefore engineered primary human T cells to express an anti-CD19 CAR currently in use clinically to treat B cell lymphomas (Kalos et al., 2011; Milone et al., 2009; June et al., 2014). We used lentiviral transduction to express the anti-CD19 CAR from mRNAs with either *WPRE*, *3'-LTR*, *TCRA* or *TCRB* 3'-UTRs to make anti-CD19 CAR T cells (**Figure 6B and 6C**). We then stimulated these CAR T cells by incubating them with CD19-expressing leukemia cells (NALM6) and measured the CAR expression by western blot analysis at different time points. Interestingly, the *TCRA* and *TCRB* 3'-UTRs induced a burst in anti-CD19 CAR protein levels within 5 hours of NALM6 cell addition, whereas the *WPRE* and *3'-LTR* sequences delayed the burst in CAR expression to ~24 hrs (**Figure 6D**). In these CAR T cells, TCR expression also followed the burst in CAR expression,

and was dependent on the presence of the CAR in addition to the NALM6 cells (**Figure 6–figure supplement 1A**). Lastly, we tested whether the timing of CAR protein expression correlates with the killing capacity of these CAR T cells. Using *in vitro* cytotoxicity assays (**Figure 6E**), CAR T cells expressing the CAR using either the *TCRA* or *TCRB* 3'-UTR showed more robust killing of two tumor cell lines compared to CARs using either the *WPRE* or *3'-LTR* 3'-UTRs (**Figure 6F–6G and Figure 6–figure supplement 1B and 1C**). This is consistent with the importance of an early burst of CAR translation for optimal CAR T cell function. These results also support the idea that using the native *TCRA* or *TCRB* 3'-UTRs for CAR expression can be used to improve CAR T cell function.

DISCUSSION

The eIF3 PAR-CLIP experiment we present here provides a snapshot of eIF3-RNA interactions that occur at the time TCR translation is most sensitive to eIF3 regulation (5 hours in Jurkat cells, **Figure 5–figure supplement 3A**). At this point in time, eIF3 crosslinks to multiple mRNAs encoding proteins involved in immune cell function (**Supplemental Files 2 and 3**). Interestingly, the patterns of eIF3 crosslinking, which for a number of mRNAs include interactions with the protein coding sequence and 3'-UTR (**Figure 1 and Figure 1–figure supplement 1G and 1H**), suggest an active role for eIF3 in promoting translation of these mRNAs. In support of this model, the two examples of pan-mRNAs we examined here (*TCRA* and *TCRB*) reside in puncta distinct from P bodies and stress granules (**Figure 1F**) and bind to eIF3 via the mRNA coding sequence on translating ribosomes (**Figure 2**). However, this eIF3-mediated translation activation is

transient, lasting only 1-2 hours in primary T cells (**Figure 5A**). Importantly, the *TCRA* and *TCRB* mRNA 3'-UTR elements are necessary and sufficient to control this burst in translation (**Figure 3**). Recent evidence suggests that eIF3 can remain associated with translating ribosomes (Bohlen et al., 2020; Lin et al., 2019; Wagner et al., 2020), a phenomenon that seems to be enhanced for the pan-mRNAs identified here. Additional layers of translation regulation also contribute to T cell function (Tan et al., 2017), particularly with respect to mTOR signaling (Miyamoto et al., 2005; Myers et al., 2019) and carbon metabolism (Manfrini et al., 2017; Ricciardi et al., 2018). The present PAR-CLIP experiments should help to elucidate additional roles for eIF3-mediated translation regulation and to map the system-wide role of translation regulation in T cell activation.

Recent experiments indicate that T cells must cross a threshold of T cell receptor signaling to commit to activation and proliferation (Au-Yeung et al., 2014, 2017), setting up a "digital" response to antigen recognition (Allison et al., 2016; Au-Yeung et al., 2014, 2017; Richard et al., 2018). The response threshold involves integration of intensity and duration of TCR signaling (Au-Yeung et al., 2014, 2017; Richard et al., 2018), and spans a wide range of TCR antigen affinity (Allison et al., 2016; Au-Yeung et al., 2014, 2017; Richard et al., 2018). Notably, T cell commitment to clonal expansion and differentiation can occur within as little as 1 to 2 hours of TCR stimulation for effector CD4+ and naive CD8+ T cells (Iezzi et al., 1998; van Stipdonk et al., 2001). Remarkably, this time period spans the burst in TCR protein synthesis mediated by eIF3 interactions with the *TCRA* and *TCRB* mRNA 3'-UTR elements (**Figure 5A**). Naive CD4+ T cells require a longer duration of TCR signaling of ~20 hours (Iezzi et al., 1998; Schrum et al., 2005). Although we were not able to distinguish levels of TCR translation in isolated CD8+ and CD4+ T

cells (**Figure 5**), subsequent events in T cell activation including CD69 and CD25 expression, and IL2 and IFNγ secretion, were equally affected in CD8+ and CD4+ cells in which the *TCRA* or *TCRB* 3'-UTR PAR-CLIP sites were deleted (**Figure 5C–5F**). In an immune response, CD28 engagement serves as the second signal required for T cell activation (Harding and Allison, 1993; Harding et al., 1992) and affects the first minutes of TCR-mediated signaling (Green et al., 1994, 2000; Michel et al., 2001; Shahinian et al., 1993; Tuosto and Acuto, 1998). Here we show CD28-mediated signaling is also needed for the burst of TCR translation on the hour timescale in primary T cells (Buckler et al., 2006) (**Figure 4**). Taken together, our results indicate that eIF3 controls *TCRA* and *TCRB* mRNA translation during the first critical hours after antigen recognition that leads to subsequent T cell commitment to proliferation and differentiation (**Figure 5**). The requirement for CD28 in PD-1 mediated inhibition of T cell activation (Hui et al., 2017; Kamphorst et al., 2017) also suggests eIF3-mediated control of TCR expression may affect PD-1 checkpoint blockade-based cancer immunotherapy (Jiang et al., 2019).

Cell immunotherapies targeting various cancers have made great strides, due to the engineering of chimeric antigen receptors that couple antigen recognition to intracellular signaling domains that activate cytotoxic T cells. However, CAR T cells often fail to eradicate cancers due to loss of activity over time, e.g. T cell exhaustion (Globerson Levin et al., 2021; Watanabe et al., 2018). Our results using nanoluciferase reporters indicated that eIF3-responsive mRNA 3'-UTR elements could be used to improve chimeric antigen receptor expression and CAR T cell responsiveness (Eyquem et al., 2017; Globerson Levin et al., 2021; Watanabe et al., 2018). We used this information to improve the ability of CAR T cells to kill tumor cells *in vitro*. With a clinically validated anti-

CD19 CAR, we found that using the *TCRA* or *TCRB* mRNA 3'-UTRs dramatically shortened the lag time before the burst in CAR protein expression upon exposure to tumor cells (**Figure 6D**). This short lag time correlated with improved tumor cell killing in cytotoxicity assays (**Figure 6E and 6F**). The burst in CAR protein expression was still not as rapid as that of the endogenous TCR in T cells stimulated by anti-CD3/anti-CD28 antibodies, however (**Figure 5A**). This could be due to multiple factors, including CAR affinity for the CD19 antigen or the activity of the 4-1BB costimulatory domain used in the present CAR (Kalos et al., 2011; Milone et al., 2009; June et al., 2014) instead of the CD28 signaling domain (Kochenderfer et al., 2009). It is also possible that the 3'-UTRs of the endogenous TCR subunits, which were left intact in the present cytotoxicity assays, and which responded to CAR signaling (**Figure 6–figure supplement 1A**), titrated cellular factors required for even shorter response times. T cell engineering to knock out the endogenous TCR or improved CAR design may shorten the lag before the burst in CAR expression and further improve CAR T cell function. Taken together, our experiments delineate the central role of eIF3 in T cell activation and highlight the importance of understanding translation regulation in immune cells to open new avenues for engineering improved cell therapies (**Figure 7**).

References and Notes:

Ahern, T., Sampson, J., and Kay, J.E. (1974). Initiation of protein synthesis during lymphocyte stimulation. Nature *248*, 519–521.

Allison, K.A., Sajti, E., Collier, J.G., Gosselin, D., Troutman, T.D., Stone, E.L., Hedrick, S.M., and Glass, C.K. (2016). Affinity and dose of TCR engagement yield proportional enhancer and gene activity in CD4+ T cells. Elife *5*.

Ascano, M., Hafner, M., Cekan, P., Gerstberger, S., and Tuschl, T. (2012). Identification of RNA-protein interaction networks using PAR-CLIP. Wiley Interdiscip. Rev. RNA *3*, 159–177.

Au-Yeung, B.B., Zikherman, J., Mueller, J.L., Ashouri, J.F., Matloubian, M., Cheng, D.A., Chen, Y., Shokat, K.M., and Weiss, A. (2014). A sharp T-cell antigen receptor signaling threshold for T-cell proliferation. Proc. Natl. Acad. Sci. U. S. A. *111*, E3679–E3688.

Au-Yeung, B.B., Smith, G.A., Mueller, J.L., Heyn, C.S., Jaszczak, R.G., Weiss, A., and Zikherman, J. (2017). IL-2 Modulates the TCR Signaling Threshold for CD8 but Not CD4 T Cell Proliferation on a Single-Cell Level. J. Immunol. *198*, 2445–2456.

Bohlen, J., Fenzl, K., Kramer, G., Bukau, B., and Teleman, A.A. (2020). Selective 40S Footprinting Reveals Cap-Tethered Ribosome Scanning in Human Cells. Mol. Cell *79*, 561–574.e5.

Boomer, J.S., and Green, J.M. (2010). An enigmatic tail of CD28 signaling. Cold Spring

542 Harb. Perspect. Biol. *2*, a002436.

543 Buckler, J.L., Walsh, P.T., Porrett, P.M., Choi, Y., and Turka, L.A. (2006). Cutting edge:
544 T cell requirement for CD28 costimulation is due to negative regulation of TCR signals
545 by PTEN. J. Immunol. *177*, 4262–4266.

546 Call, M.E., and Wucherpfennig, K.W. (2005). The T cell receptor: critical role of the
547 membrane environment in receptor assembly and function. Annu. Rev. Immunol. *23*,
548 101–125.

549 Chen, L., and Flies, D.B. (2013). Molecular mechanisms of T cell co-stimulation and co-
550 inhibition. Nat. Rev. Immunol. *13*, 227–242.

551 Choi, A.-R., Kim, J.-H., Woo, Y.H., Cheon, J.H., Kim, H.S., and Yoon, S. (2016). Co-
552 treatment of LY294002 or MK-2206 with AZD5363 Attenuates AZD5363-induced
553 Increase in the Level of Phosphorylated AKT. Anticancer Res. *36*, 5849–5858.

554 Cochran, J.R., Aivazian, D., Cameron, T.O., and Stern, L.J. (2001). Receptor clustering
555 and transmembrane signaling in T cells. Trends Biochem. Sci. *26*, 304–310.

556 Dong, D., Zheng, L., Lin, J., Zhang, B., Zhu, Y., Li, N., Xie, S., Wang, Y., Gao, N., and
557 Huang, Z. (2019). Structural basis of assembly of the human T cell receptor-CD3
558 complex. Nature *573*, 546–552.

559 Esensten, J.H., Helou, Y.A., Chopra, G., Weiss, A., and Bluestone, J.A. (2016). CD28
560 Costimulation: From Mechanism to Therapy. Immunity *44*, 973–988.

561 Eyquem, J., Mansilla-Soto, J., Giavridis, T., van der Stegen, S.J.C., Hamieh, M.,

562 Cunanan, K.M., Odak, A., Gönen, M., and Sadelain, M. (2017). Targeting a CAR to the
563 TRAC locus with CRISPR/Cas9 enhances tumour rejection. Nature *543*, 113–117.

564 Friedman, K.M., Garrett, T.E., Evans, J.W., Horton, H.M., Latimer, H.J., Seidel, S.L.,
565 Horvath, C.J., and Morgan, R.A. (2018). Effective Targeting of Multiple B-Cell
566 Maturation Antigen-Expressing Hematological Malignances by Anti-B-Cell Maturation
567 Antigen Chimeric Antigen Receptor T Cells. Hum. Gene Ther. *29*, 585–601.

568 Globerson Levin, A., Rivière, I., Eshhar, Z., and Sadelain, M. (2021). CAR T cells:
569 Building on the CD19 paradigm. Eur. J. Immunol.

570 Green, J.M., Noel, P.J., Sperling, A.I., Walunas, T.L., Gray, G.S., Bluestone, J.A., and
571 Thompson, C.B. (1994). Absence of B7-dependent responses in CD28-deficient mice.
572 Immunity *1*, 501–508.

573 Green, J.M., Karpitskiy, V., Kimzey, S.L., and Shaw, A.S. (2000). Coordinate regulation
574 of T cell activation by CD2 and CD28. J. Immunol. *164*, 3591–3595.

575 Hafner, M., Landthaler, M., Burger, L., Khorshid, M., Hausser, J., Berninger, P.,
576 Rothballer, A., Ascano, M., Jr, Jungkamp, A.-C., Munschauer, M., et al. (2010).
577 Transcriptome-wide identification of RNA-binding protein and microRNA target sites by
578 PAR-CLIP. Cell *141*, 129–141.

579 Harding, F.A., and Allison, J.P. (1993). CD28-B7 interactions allow the induction of
580 CD8+ cytotoxic T lymphocytes in the absence of exogenous help. J. Exp. Med. *177*,
581 1791–1796.

582 Harding, F.A., McArthur, J.G., Gross, J.A., Raulet, D.H., and Allison, J.P. (1992). CD28-
583 mediated signalling co-stimulates murine T cells and prevents induction of anergy in T-
584 cell clones. Nature *356*, 607–609.

585 Hernández, G., García, A., Sonenberg, N., and Lasko, P. (2020). Unorthodox
586 Mechanisms to Initiate Translation Open Novel Paths for Gene Expression. J. Mol. Biol.
587 *432*, 166702.

588 Hui, E., Cheung, J., Zhu, J., Su, X., Taylor, M.J., Wallweber, H.A., Sasmal, D.K., Huang,
589 J., Kim, J.M., Mellman, I., et al. (2017). T cell costimulatory receptor CD28 is a primary
590 target for PD-1-mediated inhibition. Science *355*, 1428–1433.

591 Huppa, J.B., and Davis, M.M. (2003). T-cell-antigen recognition and the immunological
592 synapse. Nat. Rev. Immunol. *3*, 973–983.

593 Iezzi, G., Karjalainen, K., and Lanzavecchia, A. (1998). The duration of antigenic
594 stimulation determines the fate of naive and effector T cells. Immunity *8*, 89–95.

595 Jiang, Y., Chen, M., Nie, H., and Yuan, Y. (2019). PD-1 and PD-L1 in cancer
596 immunotherapy: clinical implications and future considerations. Hum. Vaccin.
597 Immunother. *15*, 1111–1122.

598 June, C.H., Levine, B.L., Porter, D.L., Kalos, M.D., and Milone, M.C. (2014).
599 Compositions for treatment of cancer.

600 Kalos, M., Levine, B.L., Porter, D.L., Katz, S., Grupp, S.A., Bagg, A., and June, C.H.
601 (2011). T cells with chimeric antigen receptors have potent antitumor effects and can

602 establish memory in patients with advanced leukemia. Sci. Transl. Med. *3*, 95ra73.

603 Kamphorst, A.O., Wieland, A., Nasti, T., Yang, S., Zhang, R., Barber, D.L., Konieczny,
604 B.T., Daugherty, C.Z., Koenig, L., Yu, K., et al. (2017). Rescue of exhausted CD8 T
605 cells by PD-1-targeted therapies is CD28-dependent. Science *355*, 1423–1427.

606 Kieft, J.S., Zhou, K., Jubin, R., and Doudna, J.A. (2001). Mechanism of ribosome
607 recruitment by hepatitis C IRES RNA. RNA *7*, 194–206.

608 Kleijn, M., and Proud, C.G. (2002). The regulation of protein synthesis and translation
609 factors by CD3 and CD28 in human primary T lymphocytes. BMC Biochem. *3*, 11.

610 Kochenderfer, J.N., Feldman, S.A., Zhao, Y., Xu, H., Black, M.A., Morgan, R.A., Wilson,
611 W.H., and Rosenberg, S.A. (2009). Construction and preclinical evaluation of an anti-
612 CD19 chimeric antigen receptor. J. Immunother. *32*, 689–702.

613 Kochenderfer, J.N., Dudley, M.E., Carpenter, R.O., Kassim, S.H., Rose, J.J., Telford,
614 W.G., Hakim, F.T., Halverson, D.C., Fowler, D.H., Hardy, N.M., et al. (2013). Donor-
615 derived CD19-targeted T cells cause regression of malignancy persisting after
616 allogeneic hematopoietic stem cell transplantation. Blood *122*, 4129–4139.

617 Koning, F., Lew, A.M., Maloy, W.L., Valas, R., and Coligan, J.E. (1988). The
618 biosynthesis and assembly of T cell receptor alpha- and beta-chains with the CD3
619 complex. J. Immunol. *140*, 3126–3134.

620 Lamper, A.M., Fleming, R.H., Ladd, K.M., and Lee, A.S.Y. (2020). A phosphorylation-
621 regulated eIF3d translation switch mediates cellular adaptation to metabolic stress.

622 Science *370*, 853–856.

623 Lee, A.S., Kranzusch, P.J., Doudna, J.A., and Cate, J.H.D. (2016). eIF3d is an mRNA
624 cap-binding protein that is required for specialized translation initiation. Nature *536*, 96–
625 99.

626 Lee, A.S.Y., Kranzusch, P.J., and Cate, J.H.D. (2015). eIF3 targets cell-proliferation
627 messenger RNAs for translational activation or repression. Nature *522*, 111–114.

628 Lin, Y., Li, F., Huang, L., Duan, H., Fang, J., Sun, L., Xing, X., Tian, G., Cheng, Y.,
629 Yang, X., et al. (2019). eIF3 associates with 80S ribosomes to promote translation
630 elongation, mitochondrial homeostasis, and muscle health.

631 Manfrini, N., Ricciardi, S., Miluzio, A., Fedeli, M., Scagliola, A., Gallo, S., Brina, D.,
632 Adler, T., Busch, D.H., Gailus-Durner, V., et al. (2017). High levels of eukaryotic
633 Initiation Factor 6 (eIF6) are required for immune system homeostasis and for steering
634 the glycolytic flux of TCR-stimulated CD4+ T cells in both mice and humans. Dev.
635 Comp. Immunol. *77*, 69–76.

636 Mao, X., Green, J.M., Safer, B., Lindsten, T., Frederickson, R.M., Miyamoto, S.,
637 Sonenberg, N., and Thompson, C.B. (1992). Regulation of translation initiation factor
638 gene expression during human T cell activation. J. Biol. Chem. *267*, 20444–20450.

639 Meyer, K.D., Patil, D.P., Zhou, J., Zinoviev, A., Skabkin, M.A., Elemento, O., Pestova,
640 T.V., Qian, S.-B., and Jaffrey, S.R. (2015). 5’ UTR m(6)A Promotes Cap-Independent
641 Translation. Cell *163*, 999–1010.

642 Michel, F., Attal-Bonnefoy, G., Mangino, G., Mise-Omata, S., and Acuto, O. (2001).
643 CD28 as a molecular amplifier extending TCR ligation and signaling capabilities.
644 Immunity *15*, 935–945.

645 Milone, M.C., Fish, J.D., Carpenito, C., Carroll, R.G., Binder, G.K., Teachey, D.,
646 Samanta, M., Lakhal, M., Gloss, B., Danet-Desnoyers, G., et al. (2009). Chimeric
647 receptors containing CD137 signal transduction domains mediate enhanced survival of
648 T cells and increased antileukemic efficacy in vivo. Mol. Ther. *17*, 1453–1464.

649 Miyamoto, S., Patel, P., and Hershey, J.W.B. (2005). Changes in ribosomal binding
650 activity of eIF3 correlate with increased translation rates during activation of T
651 lymphocytes. J. Biol. Chem. *280*, 28251–28264.

652 Mukherjee, N., Wessels, H.-H., Lebedeva, S., Sajek, M., Ghanbari, M., Garzia, A.,
653 Munteanu, A., Yusuf, D., Farazi, T., Hoell, J.I., et al. (2019). Deciphering human
654 ribonucleoprotein regulatory networks. Nucleic Acids Res. *47*, 570–581.

655 Myers, D.R., Wheeler, B., and Roose, J.P. (2019). mTOR and other effector kinase
656 signals that impact T cell function and activity. Immunol. Rev. *291*, 134–153.

657 Ohashi, P.S., Mak, T.W., Van den Elsen, P., Yanagi, Y., Yoshikai, Y., Calman, A.F.,
658 Terhorst, C., Stobo, J.D., and Weiss, A. (1985). Reconstitution of an active surface
659 T3/T-cell antigen receptor by DNA transfer. Nature *316*, 606–609.

660 Omer, A., Peres, A., Rodriguez, O.L., Watson, C.T., Lees, W., Polak, P., Collins, A.M.,
661 and Yaari, G. (2021). T Cell Receptor Beta (TRB) Germline Variability is Revealed by
662 Inference From Repertoire Data.

Park, J.H., Rivière, I., Gonen, M., Wang, X., Sénéchal, B., Curran, K.J., Sauter, C., Wang, Y., Santomasso, B., Mead, E., et al. (2018). Long-Term Follow-up of CD19 CAR Therapy in Acute Lymphoblastic Leukemia. N. Engl. J. Med. *378*, 449–459.

de la Parra, C., Ernlund, A., Alard, A., Ruggles, K., Ueberheide, B., and Schneider, R.J. (2018). A widespread alternate form of cap-dependent mRNA translation initiation. Nat. Commun. *9*, 3068.

Pelletier, J., and Sonenberg, N. (2019). The Organizing Principles of Eukaryotic Ribosome Recruitment. Annu. Rev. Biochem. *88*, 307–335.

Qin, J.S., Johnstone, T.G., Baturevych, A., Hause, R.J., Ragan, S.P., Clouser, C.R., Jones, J.C., Ponce, R., Krejsa, C.M., Salmon, R.A., et al. (2020). Antitumor Potency of an Anti-CD19 Chimeric Antigen Receptor T-Cell Therapy, Lisocabtagene Maraleucel in Combination With Ibrutinib or Acalabrutinib. J. Immunother. *43*, 107–120.

Ricciardi, S., Manfrini, N., Alfieri, R., Calamita, P., Crosti, M.C., Gallo, S., Müller, R., Pagani, M., Abrignani, S., and Biffo, S. (2018). The Translational Machinery of Human CD4+ T Cells Is Poised for Activation and Controls the Switch from Quiescence to Metabolic Remodeling. Cell Metab. *28*, 895–906.e5.

Richard, A.C., Lun, A.T.L., Lau, W.W.Y., Göttgens, B., Marioni, J.C., and Griffiths, G.M. (2018). T cell cytolytic capacity is independent of initial stimulation strength. Nat. Immunol. *19*, 849–858.

Scaviner, D., and Lefranc, M.P. (2000). The human T cell receptor alpha variable (TRAV) genes. Exp. Clin. Immunogenet. *17*, 83–96.

684 Schrum, A.G., Palmer, E., and Turka, L.A. (2005). Distinct temporal programming of
685 naive CD4+ T cells for cell division versus TCR-dependent death susceptibility by
686 antigen-presenting macrophages. Eur. J. Immunol. *35*, 449–459.

687 Shahinian, A., Pfeffer, K., Lee, K.P., Kündig, T.M., Kishihara, K., Wakeham, A., Kawai,
688 K., Ohashi, P.S., Thompson, C.B., and Mak, T.W. (1993). Differential T cell
689 costimulatory requirements in CD28-deficient mice. Science *261*, 609–612.

690 Siefken, R., Klein-Hessling, S., Serfling, E., Kurrle, R., and Schwinzer, R. (1998). A
691 CD28-associated signaling pathway leading to cytokine gene transcription and T cell
692 proliferation without TCR engagement. J. Immunol. *161*, 1645–1651.

693 van Stipdonk, M.J., Lemmens, E.E., and Schoenberger, S.P. (2001). Naïve CTLs
694 require a single brief period of antigenic stimulation for clonal expansion and
695 differentiation. Nat. Immunol. *2*, 423–429.

696 Tan, H., Yang, K., Li, Y., Shaw, T.I., Wang, Y., Blanco, D.B., Wang, X., Cho, J.-H.,
697 Wang, H., Rankin, S., et al. (2017). Integrative Proteomics and Phosphoproteomics
698 Profiling Reveals Dynamic Signaling Networks and Bioenergetics Pathways Underlying
699 T Cell Activation. Immunity *46*, 488–503.

700 Tauber, D., Tauber, G., and Parker, R. (2020). Mechanisms and Regulation of RNA
701 Condensation in RNP Granule Formation. Trends Biochem. Sci. *45*, 764–778.

702 Thoreen, C.C., Kang, S.A., Chang, J.W., Liu, Q., Zhang, J., Gao, Y., Reichling, L.J.,
703 Sim, T., Sabatini, D.M., and Gray, N.S. (2009). An ATP-competitive mammalian target
704 of rapamycin inhibitor reveals rapamycin-resistant functions of mTORC1. J. Biol. Chem.

284, 8023–8032.

Tuosto, L., and Acuto, O. (1998). CD28 affects the earliest signaling events generated by TCR engagement. Eur. J. Immunol. *28*, 2131–2142.

Wagner, S., Herrmannová, A., Hronová, V., Gunišová, S., Sen, N.D., Hannan, R.D., Hinnebusch, A.G., Shirokikh, N.E., Preiss, T., and Valášek, L.S. (2020). Selective Translation Complex Profiling Reveals Staged Initiation and Co-translational Assembly of Initiation Factor Complexes. Mol. Cell *79*, 546–560.e7.

Wang, M., Munoz, J., Goy, A., Locke, F.L., Jacobson, C.A., Hill, B.T., Timmerman, J.M., Holmes, H., Jaglowski, S., Flinn, I.W., et al. (2020). KTE-X19 CAR T-Cell Therapy in Relapsed or Refractory Mantle-Cell Lymphoma. N. Engl. J. Med. *382*, 1331–1342.

Watanabe, K., Kuramitsu, S., Posey, A.D., Jr, and June, C.H. (2018). Expanding the Therapeutic Window for CAR T Cell Therapy in Solid Tumors: The Knowns and Unknowns of CAR T Cell Biology. Front. Immunol. *9*, 2486.

Wolf, T., Jin, W., Zoppi, G., Vogel, I.A., Akhmedov, M., Bleck, C.K.E., Beltraminelli, T., Rieckmann, J.C., Ramirez, N.J., Benevento, M., et al. (2020). Dynamics in protein translation sustaining T cell preparedness. Nat. Immunol. *21*, 927–937.

Wu, Y.-H., Huang, Y.-F., Chen, C.-C., Huang, C.-Y., and Chou, C.-Y. (2020). Comparing PI3K/Akt Inhibitors Used in Ovarian Cancer Treatment. Front. Pharmacol. *11*, 206.

Xu, Z.Z., and Mathews, D.H. (2016). Prediction of Secondary Structures Conserved in

725 Multiple RNA Sequences. Methods Mol. Biol. *1490*, 35–50.

726

Acknowledgments: We thank M. Hafner for advice on PAR-CLIP methodology and data analysis, A. Weiss for experimental suggestions and advice, H. Nolla and A. Valeros at the UC Berkeley flow cytometry facility for helping out with the FACS analysis and single cell sorting, F. Ives and H. L. Aaron at the UC Berkeley Imaging center for help with microscopy, J. Lui and J. Bohlen for advice on planning experiments and for suggestions on the manuscript, N. Aleksashin and A.M. González-Sánchez for advice on the manuscript, and M. Mignardi for advice on FISH experiments. Figure 6E and 7 were created using Biorender. com. **Funding:** This work was supported by NIH grant R01-GM065050 (J.H.D.C.) and a grant from the Tang Prize for Biopharmaceutical Science (J.H.D.C.). N.T.I. is a Damon Runyon-Rachleff Innovator (DRR#37-15) and NIH New Innovator (DP2 CA195768). A.M. holds a Career Award for Medical Scientists from the Burroughs Wellcome Fund and The Cancer Research Institute (CRI) Lloyd J. Old STAR grant and has received funding from the Chan Zuckerberg Biohub, Innovative Genomics Institute (IGI) and the Parker Institute for Cancer Immunotherapy (PICI). B.E.S. is supported by NIH grant P30EY003176. Imaging experiments were conducted at the Cancer Research Laboratory Molecular Imaging Center, supported by Helen Wills Neuroscience Institute. Sequencing was carried out at the UCSF Center for Advanced Technology and at the Vincent J. Coates Genomics Sequencing Laboratory at UC Berkeley, supported by NIH grant S10 OD018174. F.B. was supported by the Care-for-Rare Foundation and the German Research Foundation (DFG). **Author Contributions:** Project and experiments were conceived and designed by D.D.S. and J.H.D.C. D.D.S. carried out all experiments, with assistance from B.E.S. and G.H.C. for image acquisition and analysis, from T.R., R.A.A., F.B. and A.M. for primary T cell genome

editing and cell culture protocols, and from L.F., M.K., N.T.I. and J.H.D.C. for analysis of deep sequencing-based experiments. The manuscript was written by D.D.S. and J.H.D.C., with editing by all authors. **Declaration of Interests:** The authors declare competing financial interests: T.L.R. and A.M. are co-founders of Arsenal Therapeutics. A.M. is a co-founder of Spotlight Therapeutics. A.M. served on the scientific advisory board of PACT Pharma, was an advisor to Juno Therapeutics and Trizell. The Marson Laboratory has received research support from Juno Therapeutics, Epinomics, Sanofi, GlaxoSmithKline,Gilead and Anthem. A provisional patent application has been filed on some of the work presented herein. **Data and Materials Availability:** Sequencing data supporting the findings in this study have been deposited in the Gene Expression Omnibus (GEO) Database (https://www.ncbi.nlm.nih.gov/geo/), with accession codes _____. Code used to analyze the microscopy images is available on github at https://github.com/Llamero/TCR_colocalization_analysis-macro.

Supplementary Materials:

Materials and Methods

Figure supplements

Captions for Supplemental Files 1-6

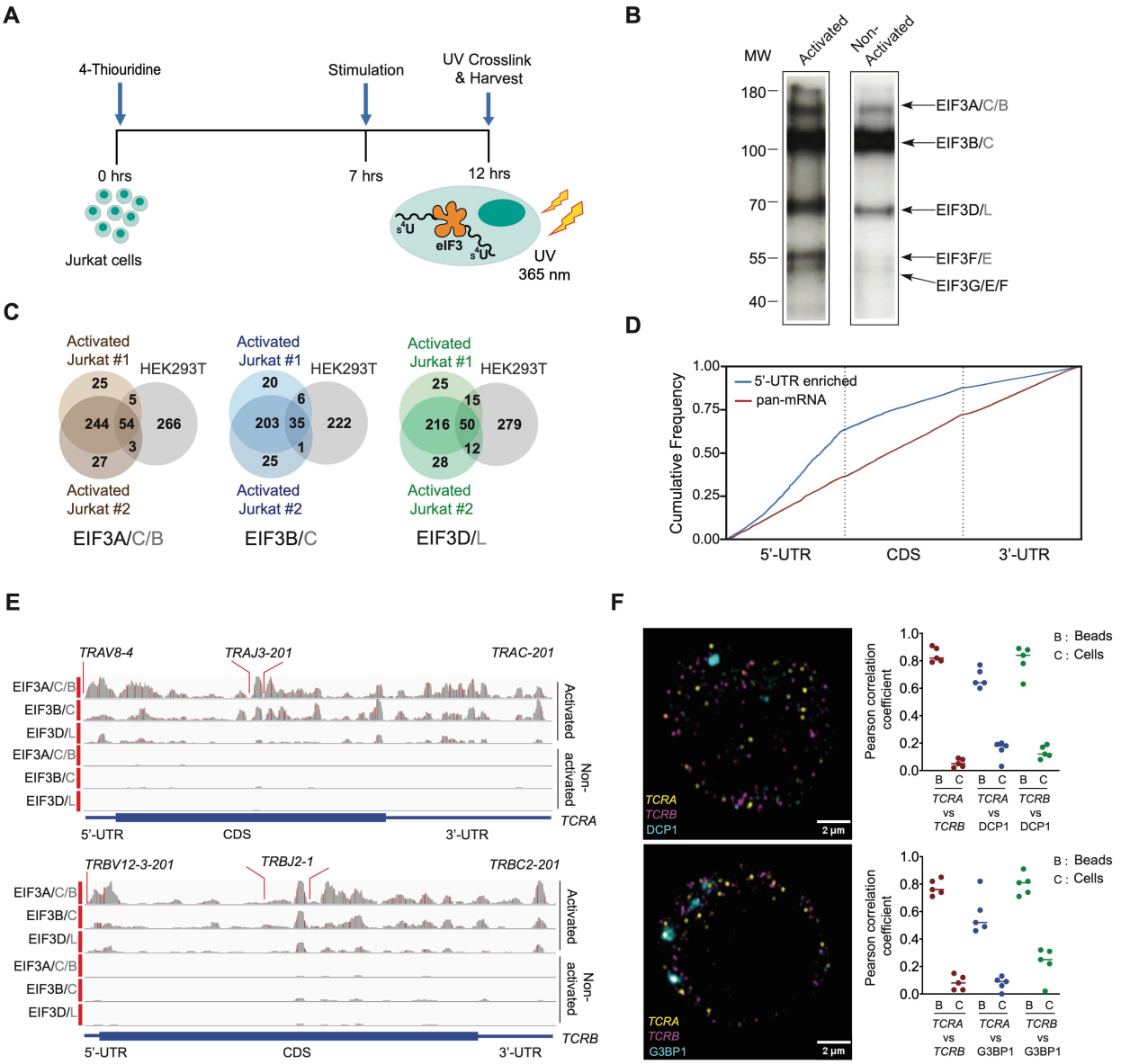

767

768 **Figure 1. eIF3 interacts with specific mRNAs related to immune function in**
769 **activated Jurkat cells.** (**A**) Schematic of the PAR-CLIP experiment in Jurkat cells,
770 showing steps through cell harvesting. (**B**) Phosphorimage of SDS polyacrylamide gel
771 resolving 5′ ^{32}P-labeled RNAs crosslinked to eIF3 subunits in activated and non-activated
772 Jurkat cells, from one of two biological replicates. (**C**) Venn diagram of genes identified
773 by eIF3 PAR-CLIP in activated Jurkat cells from two biological replicates, compared with

the eIF3 PAR-CLIP mRNAs previously identified in HEK293T cells. The same number of mRNAs from the Jurkat cell PAR-CLIP libraries, ranked by total reads mapped to a given gene, are compared to the number of mRNAs identified in the HEK293T PAR-CLIP experiments. (**D**) Varied mRNA crosslinking patterns to eIF3 in activated Jurkat cells. Cumulative plot showing mRNA crosslinking in sample EIF3A/C/B to predominantly the 5'-UTR (n = 396, 414 mRNAs in replicates 1 and 2, respectively), and across the entire length of some mRNAs ("pan-mRNAs", n = 634, 621 mRNAs). The 5'-UTR, CDS, and 3'-UTR regions are shown normalized by length. (**E**) Crosslinking of the eIF3 subunits as indicated across the entire *TCRA* and *TCRB* mRNAs, in activated and non-activated Jurkat cells. 5'-UTR, coding sequence (CDS), and 3'-UTR elements (below) along with the variable (V), joining (J) and constant (C) regions (above) for the mapped TCR genes in Jurkat cells are shown. The blue and red vertical lines in the plotted reads indicate the amount of T-C transitions vs other mutations, respectively for a particular nucleotide. The *TCRA* and *TCRB* mRNAs are present in both non-activated and activated Jurkat cells (**Supplementary File 4**). (**F**) FISH analysis of *TCRA* and *TCRB* mRNAs (yellow and magenta, respectively) and P bodies (top) marked by the location of DCP1 (cyan) and stress granules (bottom) marked by the location of G3BP1 (cyan), in activated Jurkat cells. Graphs to the right of the images indicate Pearson's correlation coefficients (PCCs) of *TCRA* and *TCRB* mRNAs localizing with each other or with P bodies or stress granules. TetraSpeck™ microsphere beads were used as a positive control for colocalization. Labels on the x axis are, B: TetraSpeck™ microsphere beads, C: activated Jurkat cells. (n = 5, P <0.008, for PCC values of cells relative to bead colocalization, across all the

796 channels tested, using the Wilcoxon rank-sum test). Images are representative of one
797 experiment of the five independent experiments in the graphs.

798

799

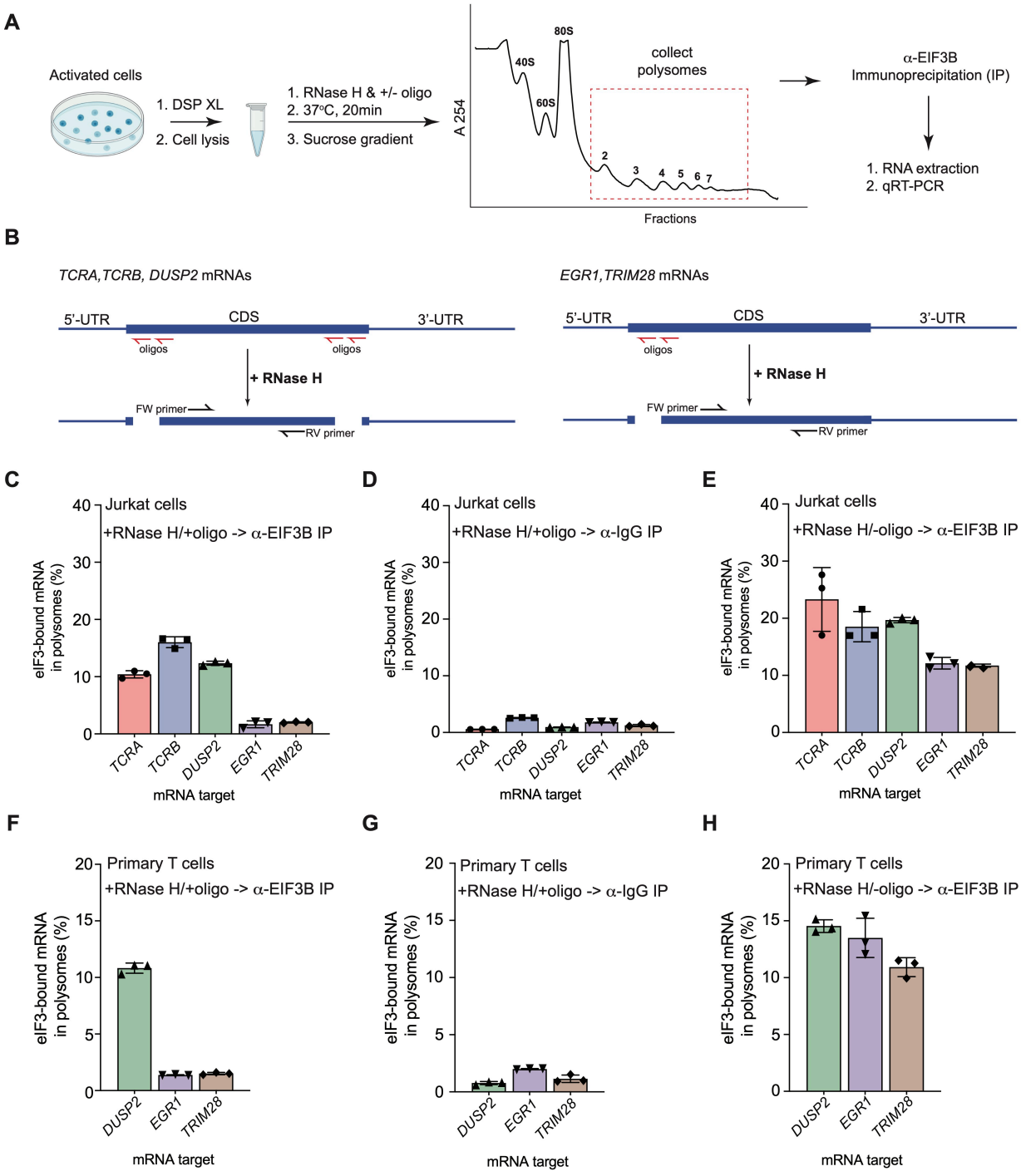

800

801 **Figure 2. eIF3 remains bound to the coding sequences (CDS) of pan-mRNAs**

802 **independent of their 5'-UTR and 3'-UTR elements in actively translating ribosomes.**

803 (**A**) Schematic outlining the RNase H-based assay of eIF3 interactions with mRNAs in

polysomes. DSP refers to the dithiobis (succinimidyl propionate) crosslinking agent. Oligos, DNA oligos designed for RNase H-mediated targeting and cleavage of specific mRNAs. (**B**) Strategy for detecting mRNA fragments released by RNase H digestion. Red arrows denote DNA oligos for RNase H-mediated targeting of mRNAs. RT-qPCR primers (black) were used to detect the CDS regions of the mRNAs. (**C**) Amount of eIF3-bound mRNA co-immunoprecipitated by an anti-EIF3B antibody (Lee et al., 2015), from polysome fractions of Jurkat cells treated with RNase H and oligos targeting the CDS-UTR junctions (red arrows diagrammed in panel **B**). (**D**) Amount of eIF3-bound mRNA co-immunoprecipitated with IgG beads, from polysome fractions of Jurkat cell lysate treated with RNase H and oligos targeting the CDS-UTR junctions. (**E**) Amount of eIF3-bound mRNA co-immunoprecipitated by the anti-EIF3B antibody, from polysome fractions of Jurkat cell lysate treated only with RNase H. (**F**) Amount of eIF3-bound mRNA co-immunoprecipitated by an anti-EIF3B antibody, from polysome fractions of primary human T cells treated with RNase H and oligos targeting the CDS-UTR junctions (red arrows diagrammed in panel **B**). (**G**) Amount of eIF3-bound mRNA co-immunoprecipitated with IgG beads, from polysome fractions of primary human T cell lysate treated with RNase H and oligos targeting the CDS-UTR junctions. (**H**) Amount of eIF3-bound mRNA co-immunoprecipitated by the anti-EIF3B antibody, from polysome fractions of primary human T cell lysate treated only with RNase H. In panels **C**–**H**, the percentage is relative to the amount of total mRNA present in the polysome fraction prior to immunoprecipitation. All the immunoprecipitation experiments in panels **C**–**H** were carried out in biological duplicate with one technical triplicate shown (n = 3, with mean

826 and standard deviations shown). The primary human T cell experiment was done using

827 2 donors.

828

829

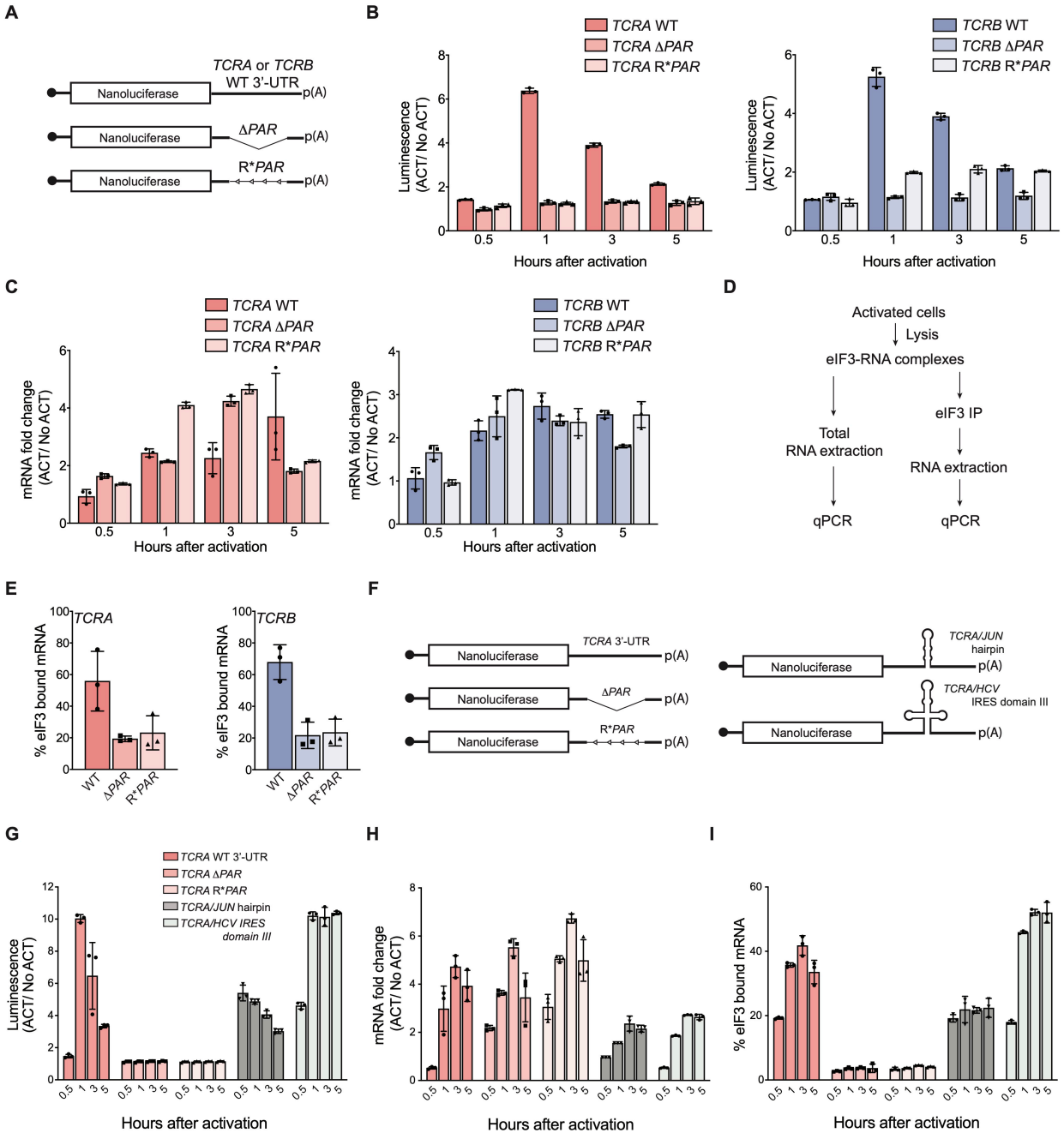

Figure 3. Interaction of eIF3 with *TCRA* and *TCRB* mRNA 3'-UTR elements mediates a burst in TCR translation in primary human T cells. (**A**) Schematic of nanoluciferase reporters stably expressed in primary human T cells. The reporters carry the *HBB* 5'-UTR and WT, *ΔPAR* or R**PAR* 3'-UTRs. WT, intact 3'-UTR from either *TCRA* or *TCRB* mRNA; *ΔPAR*, 3'-UTR of *TCRA* or *TCRB* with the eIF3 PAR-CLIP site deleted; R**PAR*, reversed

PAR-CLIP sequence in the 3'-UTR of *TCRA* or *TCRB* mRNA. (**B**) Luciferase activity in anti-CD3/anti-CD28 activated T cells stably expressing nanoluciferase constructs described in **A**, relative to non-activated controls (ACT/NoACT). (**C**) Changes in nanoluciferase mRNA levels in **B**, as determined by qRT-PCR. (**D**) Schematic of immunoprecipitation of eIF3 using an anti-EIF3B antibody (Lee et al., 2015), followed by qRT-PCR to quantify the amount of nanoluciferase mRNA bound to eIF3. (**E**) Immunoprecipitation as shown in **D** showing the amount of nanoluciferase mRNA bound to eIF3 in T cells stably transduced with either *TCRA* (left) or *TCRB* (right) WT, *ΔPAR* or R**PAR* 3'-UTRs after activation with anti-CD3/anti-CD28 antibodies for 1 hour. The percent mRNA bound to anti-EIF3B beads is calculated relative to total mRNA isolated from the cells. (**F**) Schematic of nanoluciferase reporters stably expressed in primary human T cells. Nanoluciferase reporters carry the *HBB* 5'-UTR and WT, Δ*PAR,* R**PAR* of the *TCRA* 3'-UTR, or Δ*PAR* of the *TCRA* 3'-UTR replaced with either a *JUN* 5'-UTR hairpin or hepatitis C viral (HCV) internal ribosome entry site (domain IIIabc). (**G**) Luciferase activity in anti-CD3/anti-CD28 activated T cells stably expressing nanoluciferase constructs described in **F**, relative to non-activated controls. (**H**) Changes in nanoluciferase mRNA levels in **G**, as determined by qRT-PCR. (**I**) Immunoprecipitation as shown in **D** to quantify the amount of nanoluciferase mRNA bound to eIF3 in T cells stably expressing nanoluciferase constructs in **F** after activation with anti-CD3/anti-CD28 antibodies for 0.5, 1, 3 and 5 hours. The percent mRNA bound to anti-EIF3B beads is calculated relative to total mRNA isolated from the cells. All experiments were carried out in triplicate (3 separate wells per condition), with mean and standard deviations shown.

858 All the primary human T cell experiments were performed using two donors and data from

859 one representative donor is shown.

860

861

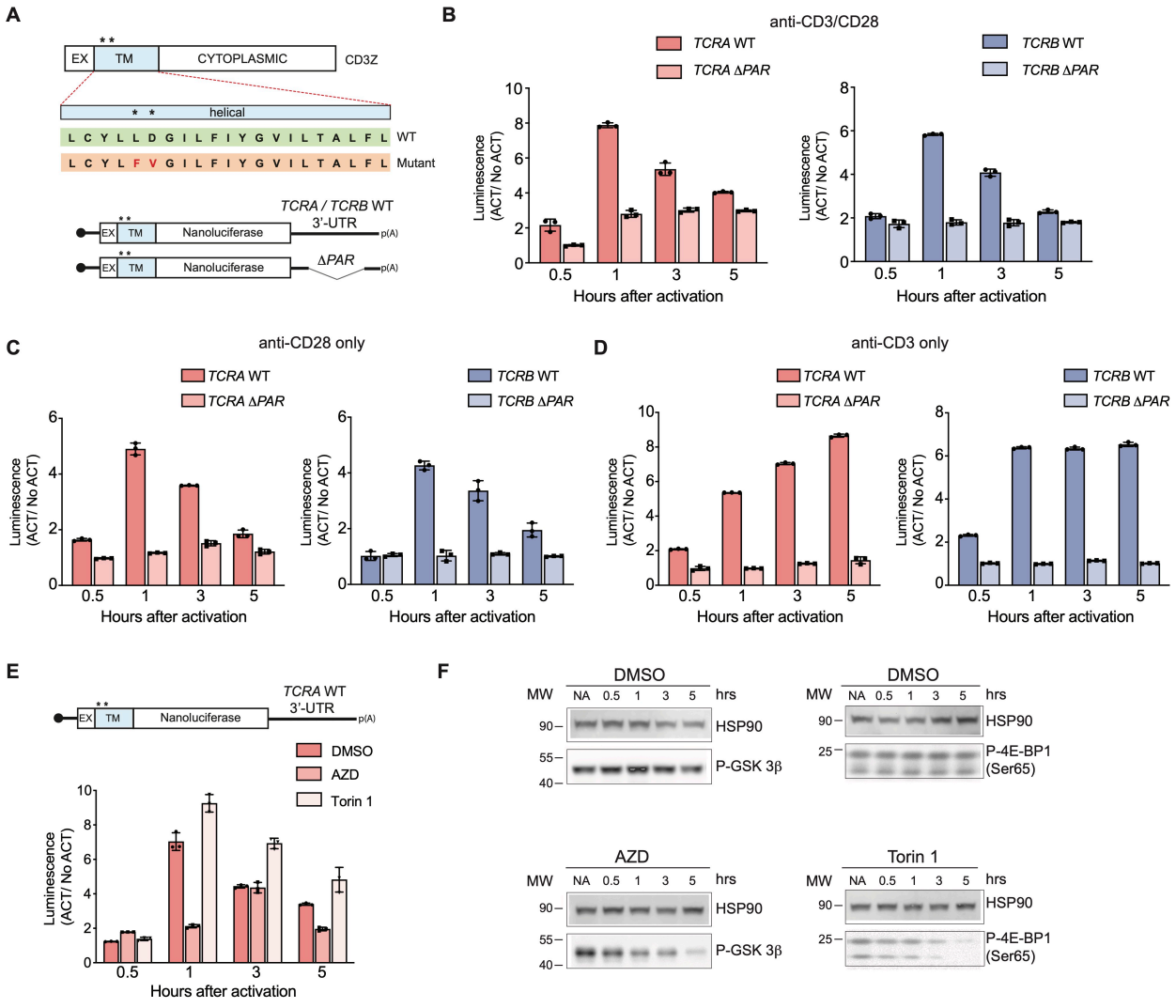

Figure 4. The burst in nanoluciferase reporter translation requires membrane-proximal CD28 signaling. (**A**) Schematic of the membrane-tethered nanoluciferase reporters stably expressed in primary human T cells. (Top) Wild-type CD3-zeta protein with asterisk indicating two amino acids mutated in the transmembrane region to prevent association with the TCR (Dong et al., 2019) (EX: extracellular, TM: transmembrane). (Bottom) Schematic of the nanoluciferase reporters. Nanoluciferase is fused C-terminal to the extracellular and transmembrane segments of CD3-zeta, mutated to prevent TCR association. The reporters carry the *HBB* 5'-UTR and *TCRA, TCRB*, *TCRA ΔPAR,* or

TCRB Δ*PAR* 3'-UTR. (**B**) Luciferase activity in primary human T cells stably expressing membrane-tethered reporters described in **A** stimulated with anti-CD3/anti-CD28 antibodies, relative to non-activated controls (ACT/NoACT). (**C**) Luciferase activity in primary human T cells stably expressing membrane-tethered reporters described in **A**, and activated only with anti-CD28 antibodies, relative to non-activated controls. (**D**) Luciferase activity in primary human T cells stably expressing membrane-tethered reporters described in **A**, and activated only with anti-CD3 antibodies, relative to non-activated controls. (**E**) Luciferase activity in primary human T cells stably expressing membrane-tethered reporter with WT *TCRA* 3'-UTR described in **A** inhibited with either AZD5363(AZD) to inhibit AKT activity or Torin 1 to inhibit mTOR before activating with anti-CD3/anti-CD28 antibodies, relative to non-activated controls. In panels **A**–**E**, all experiments were carried out in triplicate (3 separate wells per condition), with mean and standard deviations shown. (**F**) Western blot carried out to measure AKT activity in the presence of AZD5363 (AZD) using an anti-Phospho-GSK-3β antibody or mTOR activity in the presence of Torin 1 using an anti-Phospho-4EBP1 antibody, for the samples in **E**. HSP90 was used as a loading control. All the primary human T cell experiments were performed using two donors and data from one representative donor is shown.

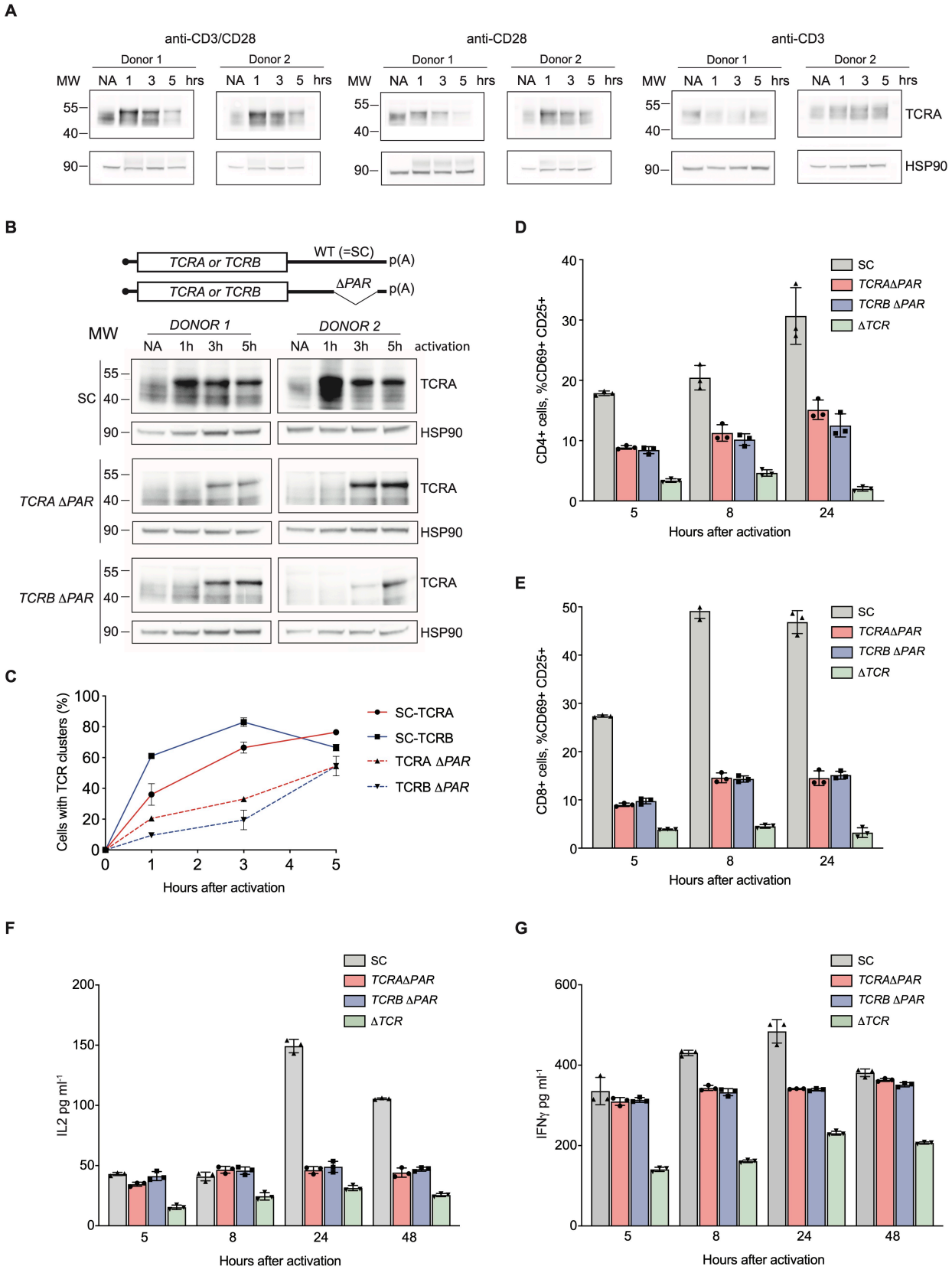

890

Figure 5. eIF3 binding to the *TCRA* and *TCRB* mRNA 3'-UTR elements is required for a rapid burst in TCR translation and robust activation of primary human T cells. (**A**) Western blots of TCRA protein levels in T cells as a function of time after different modes of activation. HSP90 was used as a loading control. (**B**) Western blots measuring TCRA protein levels as a function of time after anti-CD3/anti-CD28 activation. Cell lines used are labeled on the left: *TCRA* Δ*PAR*, *TCRB* Δ*PAR*, and SC (scrambled gRNA). HSP90 was used as a loading control. Schematics of *TCRA* and *TCRB* mRNAs with and without eIF3 PAR-CLIP sites are shown above. SC control cells have the WT 3'-UTRs for *TCRA* and *TCRB* mRNAs. (**C**) The number of T cells with one or more TCR clusters measured by anti-TCRA/anti-TCRB protein staining and epifluorescence microscopy as a function of time after anti-CD3/anti-CD28 activation. A total of 100 cells from each donor were imaged for *TCRA* Δ*PAR* (*n* = 2 donors, stained with anti-TCRA antibody), *TCRB* Δ*PAR* (*n* = 2 donors, stained with anti-TCRB antibody), and SC cell lines (*n* = 2 donors, each stained separately with anti-TCRA and anti-TCRB antibodies). Values are mean ± standard deviation. (**D**) Flow cytometric analysis measuring T cell activation markers CD69 (early activation marker) and CD25 (mid-activation marker), quantifying the mean percent of CD4+ T cells that are CD69+ CD25+. (**E**) Flow cytometric analysis of CD8+ T cells, quantifying the mean percent of CD8+ T cells that are CD69+ CD25+. Cells sorted as shown in **Figure 5–figure supplement 2**. (**F**) Quantification of IL2 secreted from SC, *TCRA* Δ*PAR, TCRB* Δ*PAR* and Δ*TCR* cell populations at different time points after stimulation with anti-CD3/anti-CD28 antibodies, as determined by ELISA. (**G**) Quantification IFNγ secreted from the cells in **F**, as determined by ELISA. In panels **D**–**G**,

913 all experiments were carried out in triplicate (3 separate wells per condition), with mean
914 and standard deviations shown. Representative results from 1 donor are shown.

915

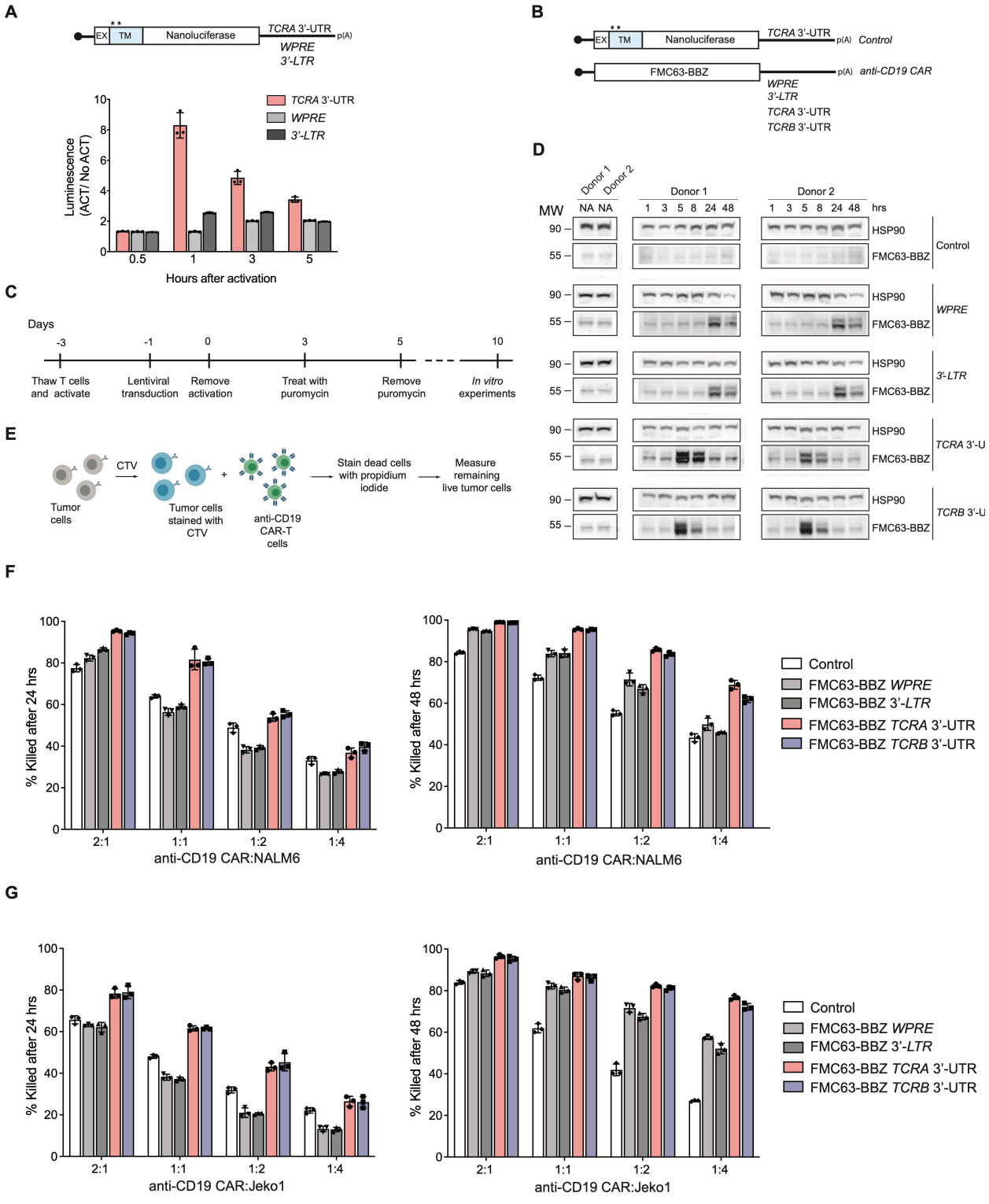

Figure 6. The *TCRA* and *TCRB* mRNA 3'-UTR elements enhance CAR T cell function. (**A**) (Top) Schematic of membrane-tethered nanoluciferase reporters stably

expressed in primary human T cells. The reporters have the *HBB* 5'-UTR and either the *TCRA* 3'-UTR, the Woodchuck Hepatitis Virus Posttranscriptional Regulatory Element (*WPRE*) or the gammaretroviral 3'-Long terminal repeat (*3'-LTR*) as 3'-UTR. (Bottom) Luciferase activity in primary human T cells stably expressing membrane-tethered nanoluciferase reporters described above and activated with anti-CD3/anti-CD28 antibodies, relative to non-activated cells. Representative results from one of two donors are shown (n = 3 separate wells, with mean and standard deviations shown). (**B**) Schematics of FMC63-BBZ CAR cDNA sequence fused 5' of the *WPRE, 3'-LTR, TCRA* 3'-UTR or *TCRB* 3'-UTR. The membrane-tethered nanoluciferase reporter with *TCRA* 3'-UTR was used as a control for the effects of lentiviral expression. (**C**) Timeline of CAR T cell generation from primary human T cells and the experiments performed. (**D**) Western blots measuring FMC63-BBZ CAR protein levels as a function of time after incubation with NALM6 cells. CAR T cells expressing the constructs in **B** are labeled: Control, *WPRE, 3'-LTR, TCRA* and *TCRB* 3'-UTR. HSP90 was used as a loading control (n = 2 donors). (**E**) Schematic describing the cytotoxicity assay used to detect live tumor cells after incubation with FMC63-BBZ CAR cells using flow cytometric analysis. (**F**) Cytotoxic activity of FMC63-BBZ CARs fused to various 3'-UTRs described in **B** after incubating with NALM6 cells for 24 and 48 hours. (**G**) Cytotoxic activity of FMC63-BBZ CARs fused to various 3'-UTRs described in **B** after incubating with Jeko 1 cells for 24 and 48 hours. In panels **F** and **G**, representative results for one of two donors are shown (n = 3 separate wells, with mean and standard deviations shown).

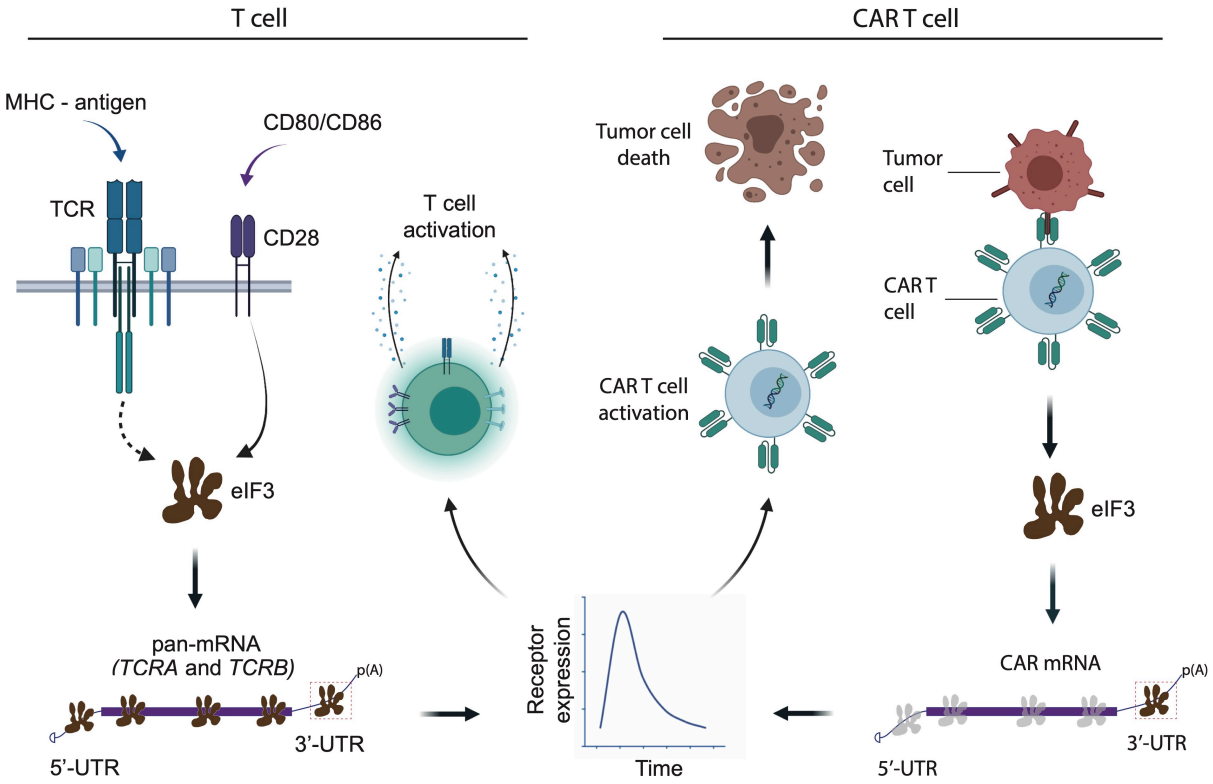

Figure 7. Model for robust T cell activation and improved CAR T cell function mediated by eIF3 interactions with the *TCRA* and *TCRB* mRNAs. Left, a T cell activated upon antigen recognition by the TCR and CD28 costimulatory signal leads to recruitment of the *TCRA* and *TCRB* mRNAs to translation "hot-spots" due to eIF3 binding to the mRNA 3'-UTRs. This results in a short burst in TCRA and TCRB translation followed by a robust increase in T cell function as measured by CD69 and CD25 expression and cytokine release. Right, activation of CAR T cells expressing CAR mRNAs with the *TCRA* or *TCRB* 3'-UTRs leads to a burst in CAR translation and improved tumor cell killing.

Supplementary Information for

Robust T cell activation requires a burst in T cell receptor translation mediated by eIF3

Authors: Dasmanthie De Silva[1,2], Lucas Ferguson[1], Grant H. Chin[1], Benjamin E. Smith[3], Ryan A. Apathy[4], Theodore L. Roth[4], Franziska Blaeschke[5], Marek Kudla[1], Alexander Marson[4,5,6,7,8,9,10], Nicholas T. Ingolia[1,11], Jamie H. D. Cate[1,2,10,11,12,13]

Correspondence to: j-h-doudna-cate@berkeley.edu

This PDF file includes:

- Materials and Methods
- Figure supplements
- Captions to Supplemental Files 1-6

Other Supplemental Information for this manuscript include the following:

- **Supplemental Files 1-6**

Materials and Methods

Jurkat cell culture

Human Jurkat, Clone E6-1 (ATCC TIB-152) was purchased from American Type Culture Collection (ATCC) and was maintained in RPMI 1640 Medium (ATCC modification) with 10% FBS (VWR Life Science Seradigm) and 0.01% Penicillin-Streptomycin (10,000 U/mL) (ThermoFisher). The cells were maintained between 1 million to 8 million cells/mL. When cells were stimulated they were always maintained at 8 million cells/mL.

Jurkat cell stimulation

The Jurkat cells used for the PAR-CLIP experiment were stimulated with 1X Cell Stimulation Cocktail, containing phorbol 12-myristate 13-acetate (PMA) and ionomycin (Thermofisher, Cat. #: 00-4970-93) to ensure a large proportion of the cells were activated. Unless otherwise stated, all other experiments involving activated Jurkat cells used anti-CD3/anti-CD28 antibodies (Tonbo) for stimulation. Flat bottom plates were coated with anti-CD3 antibody at a 10 µg/mL concentration, and anti-CD28 antibody was added to the cell culture media at a concentration of 5 µg/mL.

Isolation of human primary T cells

Primary human T cells were isolated from healthy human donors from leukoreduction chambers after Trima Apheresis (Vitalant, formerly Blood Centers of the

Pacific). Peripheral blood mononuclear cells (PBMCs) were isolated from whole blood samples by Ficoll centrifugation using SepMate tubes (STEMCELL) per manufacturer's instructions. T cells were isolated from PBMCs from all cell sources by magnetic negative selection using an EasySep Human T Cell Isolation Kit (STEMCELL), per manufacturer's instructions. Unless otherwise noted, isolated T cells were stimulated with anti-CD3/anti-CD28 antibodies (Tonbo) as described above and used immediately.

Primary human T cell culture

Bulk T cells were cultured in XVivo15 medium (Lonza) with 5% fetal bovine serum (FBS), 50 μM 2-mercaptoethanol (Sigma), and 10 μM *N*-acetyl-cystine (Sigma) or ImmunoCult™-XF T Cell Expansion Medium (StemCell). Immediately after isolation, T cells were either frozen or stimulated for 2 days with anti-human CD3/CD28 magnetic Dynabeads (ThermoFisher) at a bead to cell concentration of 1:1, along with cytokine IL-2 (UCSF Pharmacy). For T cells cultured after electroporation, the media was supplemented with IL-2 at 500 U/mL. Throughout the culture period T cells were maintained at an approximate density of 1 million cells per mL of media. Every 2–3 days after electroporation, additional media was added, along with fresh IL-2 at 500 U/mL concentration, and the cells were transferred to larger culture flasks as necessary to maintain a density of 1 million cells per mL. For all the other times T cells were maintained at 50U/mL IL-2 with the addition of fresh media every 2 days.

Primary human T cell stimulation

For edited primary human T cells, the cells were transferred to fresh media lacking IL-2 after 9 days of culturing. The T cells were then stimulated with anti-CD3/anti-CD28 antibodies using flat bottom plates coated with anti-CD3 antibody (Tonbo) at a 10 µg/mL concentration, and anti-CD28 antibody (Tonbo) added to the cell culture media at a concentration of 5 µg/mL. In all other primary human T cell stimulation experiments the cells were stimulated with anti-CD3/anti-CD28 antibodies as mentioned above along with 50 U/mL IL-2.

4-thiouridine optimization for PAR-CLIP experiments

We used Jurkat cells as a model for T cells, as PAR-CLIP experiments require a large number of cells labeled with 4-thiouridine (Sigma) at a non-toxic concentration (Ascano et al., 2012). Jurkat cells also have a defined T cell receptor and transcriptome, avoiding the donor-to-donor variability of primary T cells. Jurkat cells were seeded, so that they reached $8X10^5$ cells ml^{-1} seeding density on the day of the experiment. Varying concentrations of 4-thiouridine (s4U) were added to the cells (50 µM, 75 µM, 100 µM, or none as a negative control). The cells were then incubated for different time points: 8 hours, 10 hours, 12 hours, or 16 hours. After each incubation time cell viability was determined using the CellTiter-Glo assay (Promega), according to the manufacturer's instructions. Concentrations at which the relative luminescence in the presence of s^4U (luminescence of the s^4U treated cells/luminescence of the untreated cells) exceeded 95% were considered non-toxic. Based on these measurements, we used 50 µM of 4-thiouridine for PAR-CLIP experiments.

PAR-CLIP

Two biological replicates were used to perform PAR-CLIP analysis as described in (Lee et al., 2015), with modifications for Jurkat cells. 50 μM of 4-thiouridine was determined as non-toxic to Jurkat cells over the time course of the PAR-CLIP experiments (Ascano et al., 2012). A total of 55 million Jurkat cells seeded at 8 million cells ml^{-1} was treated with 50 μM of 4-thiouridine for 7 hours, then stimulated with 1X Cell Stimulation Cocktail for 5 hours in media containing 50 μM of 4-thiouridine (**Figure 1A**). The same number of cells were treated with 50 μM of 4-thiouridine for 12 hours without stimulation as a non-activated control. The cells were then crosslinked on ice with 365 nm UV irradiation at an energy dose of 0.2 J cm^{-2}. The cells were pelleted by centrifugation at 100 x g for 15 min at 4 °C, and the pellet was resuspended in three volumes of NP40 lysis buffer (50 mM HEPES-KOH pH 7.5, 150 mM KCl, 2 mM EDTA, 0.5% Nonidet P-40 alternative, 0.5 mM dithiothreitol (DTT), 1 Complete Mini EDTA-free Protease Inhibitor Cocktail tablet (Roche)). The cell suspension was then incubated on ice for 10 min, passed through an 18G needle five times, and centrifuged at 13,000 x g for 15 min at 4 °C and RNAs were lightly digested by treatment with MNase (Thermo Scientific) at a final concentration of 0.05 U $μl^{-1}$ for 20 min at 16 °C. For each PAR-CLIP assay 1000 μl of Dynabeads (Invitrogen) and 800 μl of anti-EIF3B antibody (Bethyl A301-761A) were used. The remaining steps of the PAR-CLIP analysis were performed exactly as described in (Danan et al., 2016; Lee et al., 2015) with the exception of using MNase at 5 U $μl^{-1}$ for the on-bead digestion step.

Mass spectrometry

To identify eIF3 subunits that crosslinked with RNAs in the PAR-CLIP experiments, a portion of eIF3 immunoprecipitated using Dynabeads as described above were treated with nonradioactive ATP (NEB) during the T4 polynucleotide kinase labeling step. The nonradioactive samples were then run on the same gel next to the radiolabeled PAR-CLIP samples, Coomassie stained (Pierce) and the bands that matched with the phosphorimager printout were excised from the gel and submitted for identification using one-dimensional LC-MS/MS (**Supplementary File 1**).

PAR-CLIP computational analysis

PAR-CLIP cDNA libraries were sequenced on an Illumina HiSeq 2500 platform. To eliminate potential PCR biases during PAR-CLIP library preparation, a random bar code was introduced into the 3' adapter and all the reads that matched the random barcode were collapsed into single reads. Clusters of overlapping sequence reads mapped against the human genome version hg38 were generated using the PARalyzer software (Corcoran et al., 2011) incorporated into the PARpipe pipeline (https://ohlerlab.mdc-berlin.de/software/PARpipe_119/, (Mukherjee et al., 2019) with the settings below. Binding sites were categorized using the Gencode GRCh38.p12 GTF annotations (gencode.v21.annotation.gtf), https://www.gencodegenes.org/human/.

The PARpipe settings used were:

Conversion = T>C

Minimum read count per group = 5

Minimum read count per cluster = 7

Minimum read count for kde = 3

Minimum cluster size = 11

Minimum conversion locations for cluster = 2

Minimum conversion count for cluster = 2

Minimum read count for cluster inclusion = 1

Minimum read length = 20

Maximum number of non conversion mismatches = 1

Comparison of eIF3 PAR-CLIP results in Jurkat and HEK293T cells

To compare RNAs in activated Jurkat cells crosslinked to eIF3 with those crosslinked to eIF3 in HEK293T cells (Lee et al., 2015), the gene cluster lists (*.gene_cl.csv) from APA_REP1, APA_REP2, APB_REP1, APB_REP2, APD_REP1, and APD_REP2 were used (see **Supplementary File 3**). The genes were first sorted by total read counts ("ReadCountSum") from high to low for each library to obtain the top candidate genes. Then, the same number of top candidate genes from these sorted lists as the number of genes identified in HEK293T cells, for eIF3 subunit EIF3A, EIF3B, and EIF3D crosslinked to RNA (Lee et al., 2015), were chosen for comparison.

PAR-CLIP Pathway analysis

To determine biological pathways enriched in the set of mRNAs that crosslinked to eIF3 in activated Jurkat cells, genes with at least 100 total aligned reads were used, as determined in the PARpipe analysis described above (Mukherjee et al., 2019), from the EIF3A/C/B samples. Since PAR-CLIP reads are short, it is not possible to determine with certainty which mRNA transcript isoform cross-linked with eIF3. Therefore the most abundant mRNA transcript isoform for each gene was chosen, as determined by transcriptome profiling using kallisto (protein_coding category) (Bray et al., 2016), as described in the Transcriptome Profiling section. Even with this choice, eIF3 crosslinks to mRNAs do not correlate with mRNA abundance (**Figure 1–figure supplement 1F**). Human genome GRCh38.p13 annotation was used to extract mRNA lengths by 5'-UTR, coding region and 3'-UTR (Ensembl Biomart) (Cunningham et al., 2019). These genes were then sorted by the density of PAR-CLIP reads in the mRNA 5'-UTR region, prior to mapping pathways of transcripts that crosslinked to eIF3. Due to the complexity of *TCRA* and *TCRB* transcript annotation, these transcripts were excluded from the normalization calculation, but included in the pathway analysis. The top 500 genes from the resulting EIF3A/C/B PAR-CLIP gene lists were used, sorted as described above, to analyze gene enrichment profiles in the STRING database (Szklarczyk et al., 2019). The top tissue-specific categories involve the immune system and T cell function (**Supplementary File 5**). Note that the STRING database categories are not mutually exclusive gene lists, and do not include TCR subunits in its analysis.

Metagene analysis

The PAR-CLIP genes sorted as described above in the "PAR-CLIP pathway analysis" were used and mapped against the most abundant mRNA transcript isoforms to generate cumulative plots of the reads. Reads for the *TCRA* and *TCRB* mRNAs were manually extracted from the Bowtie version 1.0.0 Hg38 alignment of the eIF3 PAR-CLIP reads. We did not identify reads mapped to the D segment of *TCRB* (e.g. to *TRBD2*) due to its short length of 16 nucleotides. These reads were combined with the mapped reads in the *.read.csv files generated by Parpipe. The combined reads were then sorted to extract only reads annotated as 5'-UTR, start codon, coding, stop codon, and 3'-UTR. The most abundant transcript isoform, as identified in the Transcriptome Profiling section using kallisto (described below) was used. Reads mapped to the 5'-UTR and start codon were normalized by the length of the 5'-UTR. Reads mapped to the coding region and stop codon were normalized by the length of the coding region. Finally, reads mapped to the 3'-UTR were normalized to the length of the 3'-UTR. Relative positions of the mapped reads along a metagene were computed based on the locations each mapped read fell within its respective feature. Relative positions were from -1 to 0 for the 5'-UTR, 0 to 1 for the coding region, and 1 to 2 for the 3'-UTR. 5'-UTR values were computed by multiplying the relative position by -1, whereas the 3'-UTR values were computed by adding 1 to the relative position. Coding region relative positions were unchanged.

The empirical cumulative distribution frequency function from R package ggplot2 (Wickham et al., 2016) was used to build the metagene plots from the vector of relative positions for the reads which mapped to a given set of reads. We defined mRNAs having a ratio of normalized 5'-UTR reads divided by 3'-UTR reads of 20 or more as "5'-UTR enriched" with respect to eIF3 crosslinking. All others were categorized as "pan-mRNAs,"

198 with eIF3 crosslinking across the entire length of the mRNA. The cut-off value 20 is not a
199 sharp boundary between the two categories of mRNA (**Figure 1–figure supplement 1G**).

200

201 Transcriptome Profiling

202 RNA samples were extracted from non-activated Jurkat cells or Jurkat cells activated for
203 5 hr with I+PMA, using the Direct-zol RNA Miniprep kit (Zymoresearch). The libraries were
204 prepared using TruSeq Stranded RNA LT Ribo-Zero Gold kit (Illumina) following the
205 manufacturer's instructions, with two biological replicates. Cutadapt (version 2.6) (Martin,
206 2011) with a minimum read length of 20, 5' end with a cutoff of 15 and the 3' end with a
207 cutoff of 10 in paired-end mode was used to remove adapters. RNA-seq reads were
208 pseudoaligned using kallisto v.0.46.0 run in quant mode with default parameters to
209 estimate transcript abundance (transcripts per million, TPM) (Bray et al., 2016). The
210 transcript index for kallisto was made with default parameters and GENCODE Release
211 32 (GRCh38.p13) FASTA file (Frankish et al., 2019).

212

213 RNA-FISH and immunofluorescence

214 Jurkat cells were washed with PBS, fixed with 3.7% (vol./vol.) paraformaldehyde
215 (VWR) for 10 min at room temperature and washed three times with PBS. PBS was
216 discarded and 1 ml 70% ethanol was added. The cells were incubated at 4°C for 16 hours.
217 The 70% ethanol was aspirated and the cells were washed once with 0.5 ml Stellaris RNA
218 wash buffer A (Biosearch technologies). The cells were then incubated with 100 µl
219 Stellaris hybridization buffer (Biosearch Technologies) containing Stellaris RNA FISH

probes (Biosearch Technologies) at a final concentration of 125 nM (**Supplementary File 6)** and with the relevant antibody (**Supplementary File 6**) for 16 hours at 28 °C. The cells were then washed twice with 0.5 ml Stellaris RNA wash buffer A containing secondary antibody conjugated with a fluorophore for 30 minutes at 37 °C in the dark. The second Stellaris RNA wash buffer A contained DAPI in addition to the secondary antibody. Finally the cells were washed once with 0.5 mL Stellaris RNA wash buffer B and mounted with mounting solution (Invitrogen). All high resolution images were taken using confocal ZEISS LSM 880 in Airyscan super-resolution mode, equipped withA Plan-Apochromat 63x/1.4 Oil objective (Zeiss). To measure colocalization of *TCRA* and *TCRB* mRNAs with each other or with P bodies (using DCP1 antibody, **Supplementary File 6**) or stress granules (G3BP1 antibody, **Supplementary File 6**) the cells were mounted along with 0.1 µm TetraSpeck™ microspheres (ThermoFisher) adhered to the slide according to manufacturer's instructions, to be able to account for the chromatic shift during image acquisition.

Colocalization analysis

To measure colocalization of *TCRA* and *TCRB* mRNAs with each other or with P bodies (using DCP1 antibody) or stress granules (G3BP1 antibody), immunofluorescently labelled cells (see above) were mounted along with 0.1 µm TetraSpeck™ microspheres (ThermoFisher) adhered to the slide according to manufacturer's instructions. The microspheres allowed for the correction of lateral and axial chromatic aberrations during image acquisition.

Z-stacks were acquired with 35 nm x 35 nm x 190 nm voxels on a ZEISS LSM 880 in Airyscan super-resolution mode, equipped with a Plan-Apochromat 63x/1.4 Oil objective (Zeiss). The images were then deconvolved to a lateral resolution of ≈150 nm and an axial resolution of ≈500 nm (as confirmed by observing the discrete Fourier transform of the z-stacks). After imaging a single cell, beads that were on the slide axial to the cell were imaged to measure the corresponding lateral and axial chromatic aberrations.

To quantify the relative colocalization, we developed an automated processing and analysis pipeline in ImageJ 1.52p available on github: https://github.com/Llamero/TCR_colocalization_analysis-macro. Specifically, the chromatic aberrations in the z-stacks were compensated for by registering the channels of the bead z-stack to one another, and then applying the same registration vectors to the corresponding channels in the cell z-stack (Parslow et al., 2014). Each channel of a z-stack was then thresholded to remove background in the image, and then the colocalization between each pair of images was measured using the Pearson's correlation coefficient. Samples in which any pair of channels in the bead z-stack had a correlation of less than 0.45 were removed from final analysis, as this suggested that the images had insufficient dynamic range in at least one of the channels for an accurate deconvolution.

Polysome analysis of eIF3-associated mRNAs

To isolate polysomes from Jurkat cells, the cells were seeded to reach 8 x 10^5 cells/mL on the day of harvest and then stimulated with anti-CD3/anti-CD28 antibodies as

265 described above for 5 hours. To isolate polysomes from primary human T cells, the cells
266 were seeded to reach 1 x 10^6 cells/mL on the day of harvest and then stimulated with anti-
267 CD3 and anti-CD28 antibodies as described above for 1 hour. Both Jurkat and primary
268 human T cells were treated with 100 µg ml^{-1} cycloheximide (VWR) 5 minutes before
269 harvesting. Cells were then collected into a 50 ml falcon tube and rinsed once with ice
270 cold PBS (ThermoFisher) supplemented with 100 µg ml^{-1} cycloheximide. The cells were
271 then incubated with 0.5 mM of the crosslinking reagent dithiobis (succinimidyl propionate)
272 (DSP, Thermofisher, Cat. #: PG82081) and 100 µg ml^{-1} cycloheximide in PBS at room
273 temperature for 15 minutes, with rocking. The crosslinking reagent was then removed and
274 the cells were incubated with quenching reagent (PBS, 100 µg ml^{-1} cycloheximide and
275 300 mM Glycine(Sigma)) for 5 minutes on ice. The cells were then rinsed again with ice
276 cold PBS and flash frozen in liquid nitrogen.

277 A total of 4 x 10^8 cells were lysed with 400 µl hypotonic lysis buffer (10 mM Hepes
278 pH 7.9, 1.5 mM $MgCl_2$, 10 mM KCl, 0.5 mM DTT, 1% Triton, 100 µg ml^{-1} cycloheximide,
279 and one Complete EDTA-free Proteinase Inhibitor Cocktail tablet (Roche)). The cells
280 were incubated for 10 min on ice and then passed through an 18G needle five times, and
281 centrifuged at 13,000 × g for 15 min at 4 °C. The 400 µl supernatant was then transferred
282 to a fresh eppendorf tube and subjected to RNase H digestion by adding the following
283 reagents: 3 mM $MgCl_2$, 10 mM DTT, 200 units RNase H (NEB) and 20 µl of SUPERasIN
284 (ThermoFisher), with a total of 4 µM DNA oligos (IDT), as indicated in the figure legends.
285 The mixture was then incubated at 37 °C for 20 minutes. After incubation 10 µl of the
286 RNase H treated lysate mixture was isolated to test the efficiency of the RNase H
287 digestion using qRT-PCR (**Figure 2–figure supplement 1B, 1D, and 1G**) and the rest of

the lysate was layered onto a 12 ml 10%-50% sucrose gradient, made with gradient buffer consisting of: 10% sucrose (w/v) or 50% sucrose (w/v), 100 mM KCl, 20 mM Hepes pH 7.6, 5 mM $MgCl_2$, 1 mM DTT and 100 µg ml^{-1} cycloheximide. The gradient was centrifuged at 36,000 rpm (222k x g) for 2 hours at 4 °C in a SW-41 rotor. The gradient was then fractionated using the Brandel gradient fractionator and ISCO UA-6 UV detector and all the polysome fractions (~ 5 ml) were collected into a fresh 15 ml falcon tube. 100 µl from each of the polysome fractions was kept aside to measure the input RNA amounts, and the rest of each polysome fraction was incubated with 100 µl of Dynabeads (Invitrogen) conjugated with 40 µl of anti-EIF3B antibody (Bethyl A301-761A) for 16 hours, rotating at 4 °C. After incubation, the beads were rinsed three times with 1000 µl room temperature NP40 lysis buffer (defined in the PAR-CLIP section), rotating for 5 minutes for each wash. After the final wash the beads were resuspended in 400 µl of Trizol (Thermofisher), the RNA was extracted and qRT-PCR was performed as described above.

Western Blot

Western blot analysis was performed using the antibodies listed in **Supplementary File 6**.

Total mRNA isolation and quantitative RT-PCR analysis

Total RNA was isolated from whole cells for qRT-PCR using Quick RNA miniprep plus kit from Zymo Research following the manufacturer's instructions. Quantitative RT-PCR analysis was performed using the Power SYBR Green RNA-to-Ct 1-Step kit (Applied

Biosystems) according to the manufacturer's instructions, and the QuantStudio™ 3 Real-Time PCR System (ThermoFisher). Each target mRNA was quantified in three biological replicates, with each biological replicate having three technical replicates.

Plasmids

Nanoluciferase reporters (Hall et al., 2012) were constructed using the 5'-UTR of the human beta globin mRNA (*HBB*) and a PEST destabilization domain. The PEST domain reduces protein half-life (Voon et al., 2005) and was used to provide better time resolution of nanoluciferase expression after T cell activation. The *TCRA* 3'-UTR and *TCRB* 3'-UTR sequences were amplified from Jurkat genomic DNA. The nanoluciferease sequence fused to a PEST domain was amplified from pNL1.2[*NlucP*] Vector Sequence (Promega) and was cloned into a modified CD813A vector (System Biosciences) using the In-Fusion® HD Cloning Kit (Takara). The subsequent mutations in the *TCRA* and *TCRB* 3'-UTRs were generated using these initial constructs. For *TCRA* Δ*PAR* constructs, nucleotides 102-338 in the 3'-UTR of *TCRA* mRNA were deleted. For *TCRB* Δ*PAR* constructs, nucleotides 16-161 in the 3'-UTR of *TCRB* mRNA were deleted. *TCRA/TCRB* Δ*PAR*, *TCRA/TCRB R*PAR, 3'-LTR* (3'-Long Terminal Repeat), *JUN* 5'-UTR hairpin (**Supplementary File 6**) and HCV IRES domain III (**Supplementary File 6**) sequences were purchased as gblocks from IDT and were cloned into this plasmid backbone. The *WPRE* (Woodchuck Hepatitis Virus Posttranscriptional Regulatory Element) 3'-UTR sequence was amplified from the CD813A-1 (System Biosciences) vector.

For nanoluciferase reporters designed to be membrane-tethered, we fused the N-terminal sequence of CD3-zeta spanning the transmembrane helix (amino acids 1-60) ordered as a gblocks from IDT to the nanoluciferase sequence above. To prevent interaction of the CD3-zeta-nanoluciferase fusion protein with the TCR, we made mutations in the CD3-zeta derived transmembrane helix that would disrupt interactions with the TCR, based on the cryo-EM structure of the complex (Dong et al., 2019) (PDB entry 6JXR) and consistent with earlier biochemical results (Call et al., 2002). The two mutations, L35F and D36V, are predicted to introduce a steric clash and disrupt an intra-membrane salt bridge, respectively, with other subunits in the TCR holo-complex. These CD3-zeta-nanoluciferase chimeras were cloned into the modified CD813A plasmids described above.

Generation of primary human T cells stably expressing nanoluciferase reporters

For lentiviral production, HEK293T cells were plated at a density of 80% in T-75 flasks the night before transfection. The cells were then transfected with plasmids: expressing the nanoluciferase, PsPAX2 and pCMV-VSV-G using the Lipofectamine 2000 reagent (ThermoFisher) following the manufacturer's instructions. Forty-eight hours after transfection, the viral supernatant was collected, filtered and concentrated using PEG-it Virus Precipitation Solution (System Biosciences) following the manufacturer's instructions. The virus pellets were then resuspended in ImmunoCult™-XF T Cell Expansion media and stored in -80 °C.

The primary human T cell transductions were done with multiple viral titers using TransDux™ MAX Lentivirus Transduction Reagent (System Biosciences) following the manufacturer's instructions. To test the viral transduction efficiency of the cells, forty-eight hours after viral transduction the percent of cells expressing GFP was measured by FACS analysis and cells expressing less than 30% GFP were treated with 1 μg ml^{-1} puromycin (ThermoFisher) for 4 days or until ~90% of the cells are GFP positive.

Luciferase reporter assays

The stable cell lines expressing the Nanoluciferase reporters were stimulated with anti-CD3/anti-CD28 antibodies with 50 U/mL IL-2 and the nanoluciferase activity was assayed after 30 min, 1 hr, 3 hr, and 5 hr after stimulation using Nano-Glo® Luciferase Assay System (Promega). For each time point 200,000 cells were tested in triplicate for each cell line.

For assays of TCR and CD28 signaling requirements, the stable cell lines were stimulated with anti-CD3 or anti-CD28 antibodies individually in the presence of 50 U/mL IL-2, and assayed as described above. To identify signaling pathways downstream of CD28, cells were incubated with AKT inhibitor AZD5363 at 1 μM (Cayman Chemical), mTOR inhibitor Torin1 250 nM (Cayman Chemical) or DMSO for 3 hours prior to T cell activation with anti-CD3/anti-CD28 antibodies (Tonbo) as indicated above. The cells were assayed as described above, and the extent of AKT and mTOR inhibition were determined by western blot analysis of phosphorylation of their substrates GSK-3β and 4E-BP1, respectively.

375

376 RNA immunoprecipitation and qPCR

377 The EIF3B-RNA immunoprecipitations were carried out following the exact same
378 conditions used for the PAR-CLIP analysis with the following changes. For each
379 immunoprecipitation, cell lysates were prepared in NP40 lysis buffer (defined in the PAR-
380 CLIP section) with 4 million cells. The lysates were then incubated with 50 µl Protein G
381 Dynabeads conjugated with 20 µl of anti-EIF3B antibody (Bethyl A301-761A) for two
382 hours at 4 °C. After incubation, the flow through was removed and the beads were washed
383 three times with 1 ml NP40 lysis buffer for each wash. The beads were then resuspended
384 in 400 µl TRIzol reagent (ThermoFisher) and vortexed for 1 minute. The RNA was
385 extracted following the manufacturer's instructions and qPCR was performed as
386 described above using primers listed in **Supplementary File 6**.

387

388 sgRNA/Cas9 RNP production

389 The sgRNA/Cas9 RNPs used to edit Jurkat cells were produced by complexing
390 sgRNA (Synthego) to Cas9 as described (Schumann et al., 2015) while RNPs to edit
391 Primary Human T cells were produced by complexing a two-component gRNA (crRNA
392 and tracrRNA, Dharmacon) to Cas9 as described in (Roth et al., 2018). The targeting
393 sequences for the sgRNAs and crRNA are given in **Supplementary File 6**. Recombinant
394 Cas9-NLS was obtained from MacroLab in the California Institute for Quantitative
395 Biosciences.

396

Primary T cell and Jurkat genome editing

Jurkat cells used for electroporation were collected at passage 5 or lower and were maintained at a seeding density of 8 million cells/mL or lower. Primary T cells were isolated as described above. Prior to electroporation the Primary T cells were stimulated with magnetic anti-CD3/anti-CD28 Dynabeads (ThermoFisher) for 48 hours. After 48 hours these beads were removed from the cells by placing cells on an EasySep cell separation magnet for 2 min before electroporation. One million Jurkat (not activated) or primary T cells cells (activated with anti-CD3/anti-CD28 Dynabeads for 48 hours) were rinsed with PBS and then resuspended in 20 µl of Lonza electroporation buffer P3. The cells were then mixed with 2.5 µl Cas9 RNPs (50 pmol total) along with 2 µl of a 127-nucleotide non-specific single-stranded DNA oligonucleotide at 2 µg μl^{-1} (4 µg ssDNA oligonucleotide total). The cells were then electroporated per well using a Lonza 4D 96-well electroporation system with pulse code DN100 for Jurkat cells and EH115 for primary human T cells. Immediately after electroporation, 80 µl of pre-warmed media (without cytokines) was added to each well, and the cells were allowed to rest for 15 min at 37 °C in a cell culture incubator while remaining in electroporation cuvettes. After 15 min, cells were moved to final culture flasks. Jurkat cells were clonally selected by single cell sorting into U-bottomed 96 well plates and by testing each clone using PCR primers flanking the editing site (**Figure 5–figure supplement 1A**). The clones producing a single PCR band of 1283 bp and 1022 bp were selected as clonal populations for *TCRA* Δ*PAR* and *TCRB* Δ*PAR* respectively.

Genome edited populations of primary T cells with the *TCRA* Δ*PAR* and *TCRB* Δ*PAR* mutations were determined by measuring the density of the PCR bands described

above resulting from the edited cell population compared to the PCR band from non edited cells, using ImageJ. To compare with the *TCRA* Δ*PAR* or *TCRB* Δ*PAR* primary T cell populations, we edited cells from both donors using each gRNA targeting the *TCRA* 3'-UTR and *TCRB* 3'-UTR region separately (single gRNA experiments), a gRNA targeting the coding sequence (CDS) of *TCRA* which knocks out TCR expression with high efficiency (Δ*TCR*) (Roth et al., 2018), a scrambled gRNA (SC) which does not target any site in the human genome, and cells mixed with the gRNA/Cas9 RNPs but not nucleofected.

Analysis of TCR cluster formation

WT, *TCRA ΔPAR* or *TCRB ΔPAR* T cells were activated with anti-CD3/anti-CD28 antibodies for 1, 3 or 5 hours, as described above. Cells were collected and stained with anti-TCRA antibodies, followed by a secondary antibody Alexa Fluor 488 goat anti-mouse IgG (Invitrogen). For the counting of cells containing TCR clusters, immunofluorescent imaging was performed on a Revolve Epi-Fluorescence microscope (Echo), equipped with an A Plan-Apochromat 40x objective (Olympus). Cells with substantial puncta (arrows in **Figure 5–figure supplement 1C**) were scored as having TCR cluster formation (**Figure 5C**).

Flow cytometry and cell sorting

Flow cytometric analysis was performed on an Attune NxT Acoustic Focusing Cytometer (ThermoFisher). Surface staining for flow cytometry and cell sorting was

performed by pelleting cells and resuspending in 50 µl of FACS buffer (2% FBS in PBS) with antibodies at a 1:100 concentration (**Supplementary File 4**) for 20 min at 4 °C in the dark. Cells were washed twice in FACS buffer before resuspension and analysis.

ELISA

The cell culture supernatants were collected after each time point of activation with anti-CD3/anti-CD28 antibodies for WT, *TCRA ΔPAR* or *TCRB ΔPAR* cells. For each timepoint the same number of cells were used from each strain to be able to compare across strains and time points. The amount of secreted IL-2 in the cell suspensions after activation anti-CD3/anti-CD28 antibodies for WT, *TCRA ΔPAR* or *TCRB ΔPAR* cells were measured by ELISA MAX™ Deluxe Set Human IL-2 (BioLegend) according to the manufacturer's instructions.

Chimeric antigen receptor (CAR) construct sequences

The CDS region of the Juno anti-CD19 chimeric antigen receptor presently used in the clinic (June et al., 2014; Kalos et al., 2011) was cloned into CD813A lentiviral vectors (Systems Biosciences) with a common core EF1alpha promoter and 5'-UTR with an inserted intron. The CDS sequence was followed by various 3'-UTRs. Two of the 3'-UTRs are presently used in clinical CAR T cells, the Woodchuck Hepatitis Virus Posttranscriptional Regulatory Element (*WPRE*) (June et al., 2014; Milone et al., 2009), or the murine stem cell virus (MSCV) retroviral 3'-long terminal repeat (*3'-LTR*)

(Kochenderfer et al., 2009). We also cloned the full *TCRA* or *TCRB* 3'-UTR sequences including the polyadenylation sites after the anti-CD19 CAR CDS sequence.

Production of CAR T cells

Production of the CAR-expressing lentiviruses was carried out as described above using HEK293T cells. The viruses were then concentrated using PEG-it Virus Precipitation Solution (System Biosciences) following the manufacturer's instructions. The virus pellets were then resuspended in ImmunoCult™-XF T Cell Expansion media and stored in -80 °C. Frozen primary human T cell pellets were thawed and then stimulated with ImmunoCult™ Human CD3/CD28/CD2 T Cell Activator (Stemcell) for 48 hours and then transduced with various CAR viruses using TransDux™ MAX Lentivirus Transduction Reagent (System Biosciences) as described above. Two days after transduction the percent of cells expressing GFP was measured by FACS analysis and cells expressing less than 30% GFP were treated with 1 μg mL^{-1} puromycin (ThermoFisher) for 2 days or until ~90% of the cells are GFP positive. After removal of puromycin the cells were seeded at $1x10^6$ cells/mL upto 9 days from the day the cells were transduced by adding fresh ImmunoCult™-XF T Cell Expansion Medium (StemCell) and 50 U/mL IL-2 every other day. After 9 days the CAR T cells were used for various assays.

CAR expression dynamics

To measure CAR expression dynamics by western blot analysis, CAR T cells were incubated with NALM6 tumor cells at a ratio of 1:2 CAR T cell:NALM6 cells, in ImmunoCult™-XF T Cell Expansion Medium (StemCell) and 50 U/mL IL-2. Cells were collected at the indicated time points and processed for western blot analysis as described above. The total protein expression level of the anti-CD19 CAR was detected with an anti-CD3z antibody (Santa Cruz Biotechnology).

CAR T-cell cytotoxicity assays

CAR T cell cytotoxicity was determined using a FACS based assay. First, NALM6 or Jeko 1 tumor cells were stained with CTV (CellTrace™ Violet, thermofisher). Cells were resuspended in 10 mL PBS (5 x 10^6 cells), 5 µl CTV was added, and the cells were incubated for 20 minutes at 37 °C. After incubation, 30 mL of RPMI media was added and the cells incubated for an additional 5 minutes at 37 °C. The cells were then gently pelleted, rinsed and resuspended in fresh ImmunoCult™-XF T Cell Expansion Medium (StemCell) and 50 U/mL IL-2. Then in a round bottom 96-well plate, 20,000 stained tumor cells were cocultured with CAR T cells at different effector-target ratios in a total volume of 200 µL for 24 hours, 48 hours and 72 hours. T cells transduced with a membrane-tethered nanoluciferase reporter containing the *TCRA* 3'-UTR (**Figure 4B**) were used as a negative control. The CAR T cell killing capacity was measured by Flow Cytometry as diagrammed in **Figure 6–figure supplement 1B**. Briefly, the 96-well plates were incubated at 4 °C for 30 minutes to terminate the killing by CAR T cells. Then 2 µL of propidium iodide (1000x stock, Thermofisher) was added

508 to each column in the plate one by one and the living tumor cells were measured as

509 shown in **Figure 6–figure supplement 1B**.

510

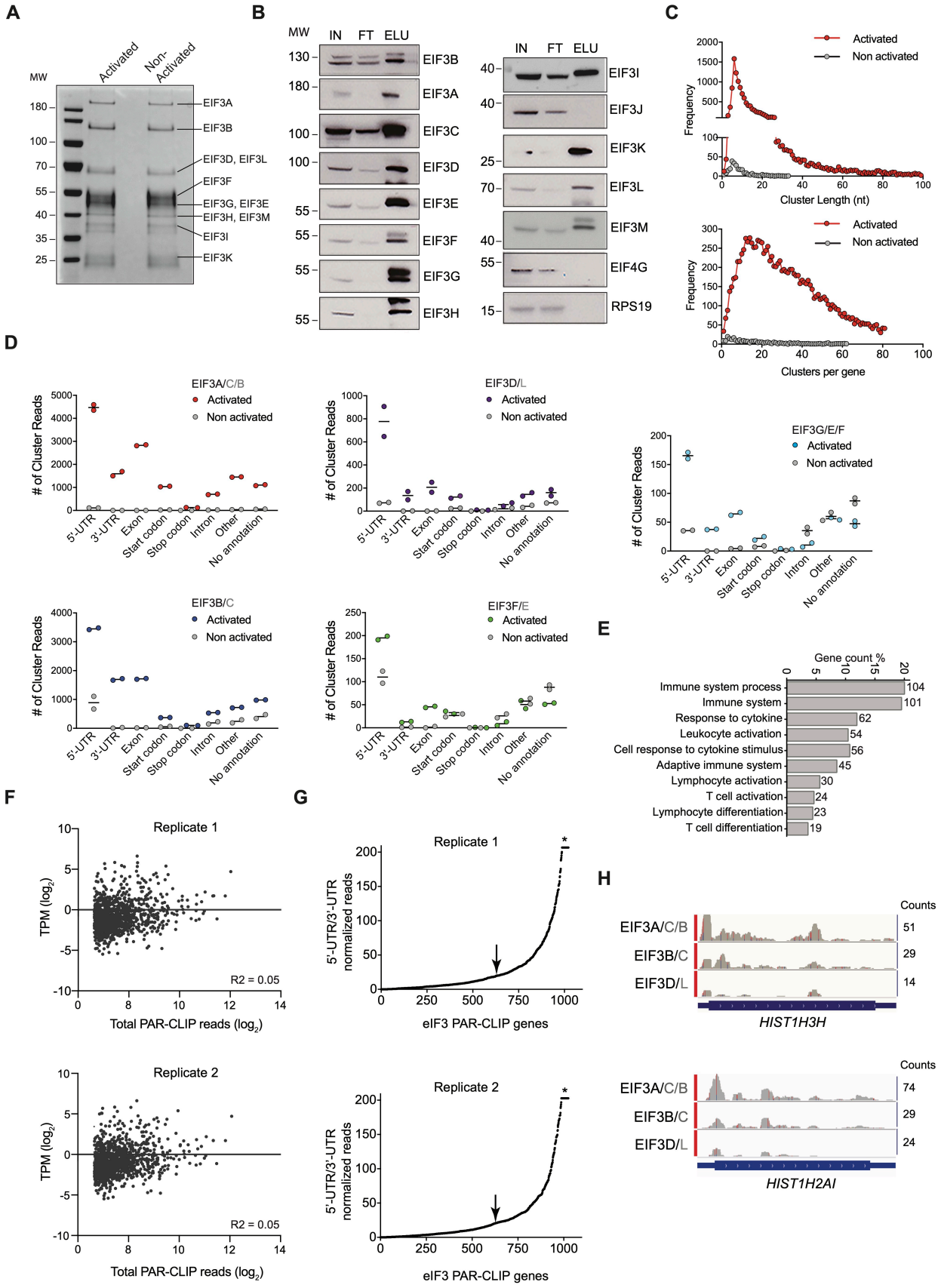

511

Figure 1–figure supplement 1. eIF3 PAR-CLIP experiments in activated and non-activated Jurkat cells. (**A**) Composition of eIF3 in I+PMA activated and non-activated Jurkat cells after anti-EIF3B immunoprecipitation (IP), identified by mass spectrometry. Shown is an SDS polyacrylamide gel stained with Coomassie Brilliant Blue. (**B**) Composition of eIF3 in activated Jurkat cells determined by western blot after anti-EIF3B IP. IN: input; FT: flow-through from anti-EIF3B IP beads; ELU: elution of eIF3 from anti-EIF3B IP beads. Anti-EIF4G1 and anti-RPS19 western blots confirm the stringency of bead wash steps (Lee et al., 2015). (**C**) (Top) The length distribution of PAR-CLIP clusters mapped to RNAs crosslinked to eIF3 in the EIF3A/C/B samples, from activated (red) and non-activated (grey) Jurkat cells. (Bottom) The frequency distribution of the number of eIF3 PAR-CLIP clusters mapped to RNAs in the EIF3A/C/B samples, from activated (red) and non-activated (grey) Jurkat cells. In all panels, the distributions are the average of both biological replicates. RNA PAR-CLIP properties observed in the EIF3A/C/B sample are representative of those seen in PAR-CLIP sequence reads of RNAs crosslinked to other eIF3 subunits. (**D**) Categories of RNA crosslinked to eIF3, defined by clusters and divided into RNA categories, in I+PMA activated Jurkat cells and non-activated Jurkat cells (grey). In all panels, RNA categories include: 5'-UTR, 5'-UTR of mRNA; 3'-UTR, 3'-UTR of mRNA; CDS, protein coding region of mRNA; Start codon, beginning of mRNA CDS; Stop codon, stop codon region of mRNA; Intron, regions of pre-mRNA; Other, other classes of RNA; No annotation, reads that map to the human genome but that have no annotation assigned. A given mRNA may give rise to clusters in different mRNA categories. (**E**) Pathway enrichment categories determined using the STRING Database for both biological replicates of the EIF3A/C/B PAR-CLIP libraries (mRNAs with >= 100

reads). Number of genes in each pathway whose mRNAs crosslinked to eIF3 is shown next to each bar. Note that the categories reported by the STRING Database are not disjoint sets. Panels **C** through **E** show representative results from one of two biological replicates. (**F**) Scatterplot of TPM of mRNAs expressed in activated Jurkat cells (most abundant isoform, see Methods) versus mRNAs identified by PAR-CLIP as crosslinked to eIF3 in the EIF3A/C/B samples, with ≥ 100 total read counts. n=1,029 and 1,035 for PAR-CLIP hit genes plotted for replicates 1 and 2, respectively. The R-squared goodness of fit to a linear equation is shown. (**G**) mRNAs sorted by increasing value of the ratio of normalized 5'-UTR reads to normalized 3'-UTR reads in the EIF3A/C/B samples. Values of the ratio of 5'-UTR/3'-UTR normalized reads > 200 have been truncated to a value of 200 in the plot (asterisk). The arrow indicates the threshold used to create cumulative plots shown in **Figure 1D**. (**H**) Examples of eIF3 crosslinking to histone mRNAs *HIST1H2AI* and *HIST1H3H* in activated Jurkat cells are shown. Transcription start sites were determined from the FANTOM5 Database (Noguchi et al., 2017).

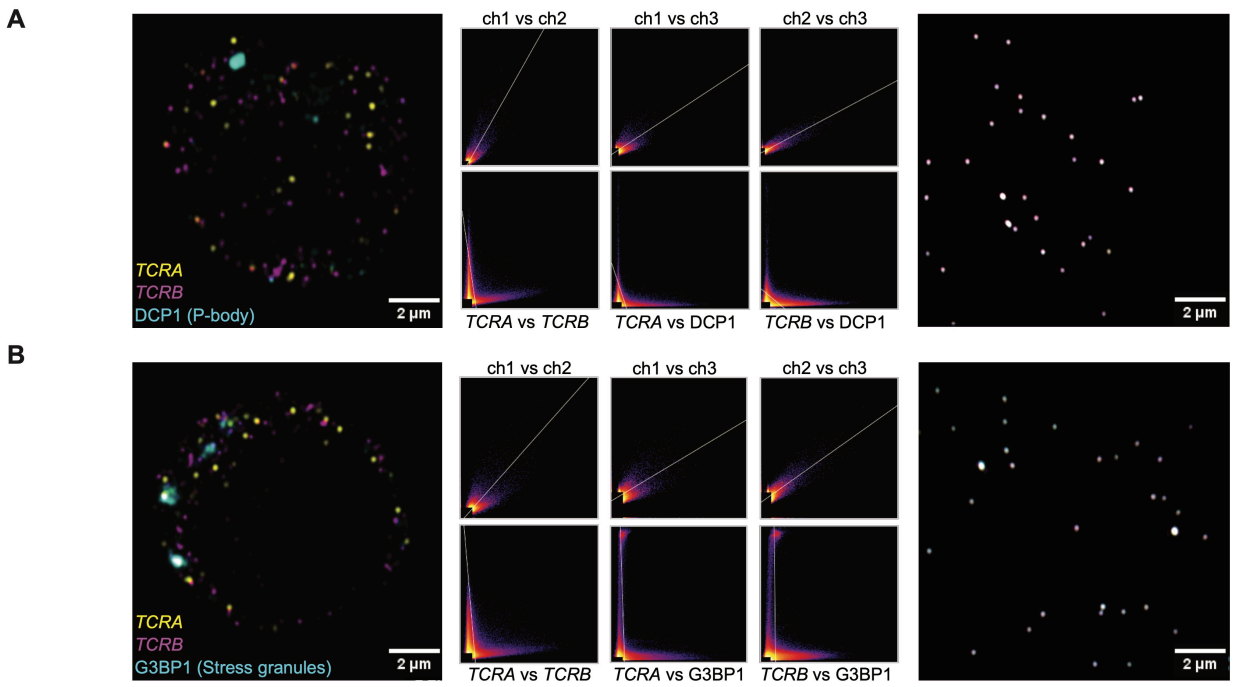

Figure 1–figure supplement 2. The *TCRA* and *TCRB* mRNAs form localized puncta in activated T cells. (**A**) (right panel) Single optical section of TetraSpeck microspheres (0.1 µm) adjacent to a Jurkat cell probed for P bodies. Scatter plots of pixel intensities in different emission channels are shown: channel 1, 670 nm; channel 2, 570 nm; channel 3, 488 nm. (left panel) Single optical section of a Jurkat cell probed for *TCRA* mRNA (channel 1), *TCRB* mRNA (channel 2), and DCP1 to mark P bodies (channel 3). (middle panels) Scatter plots showing : channel 1 vs. channel 2, channel 1 vs. channel 3, and channel 2 vs. channel 3. (**B**) (right panel) Single optical section and scatter plots for TetraSpeck microspheres as in **A**, but adjacent to a Jurkat cell probed for stress granules. (left panel) Single plane image of a Jurkat cell probed for *TCRA* mRNA (channel 1), *TCRB* mRNA (channel 2), and G3BP1 to mark stress granules (channel 3). (middle panels) Scatter plots as in **A**. Images of each cell are representative of those used in the analysis in **Figure 1F**.

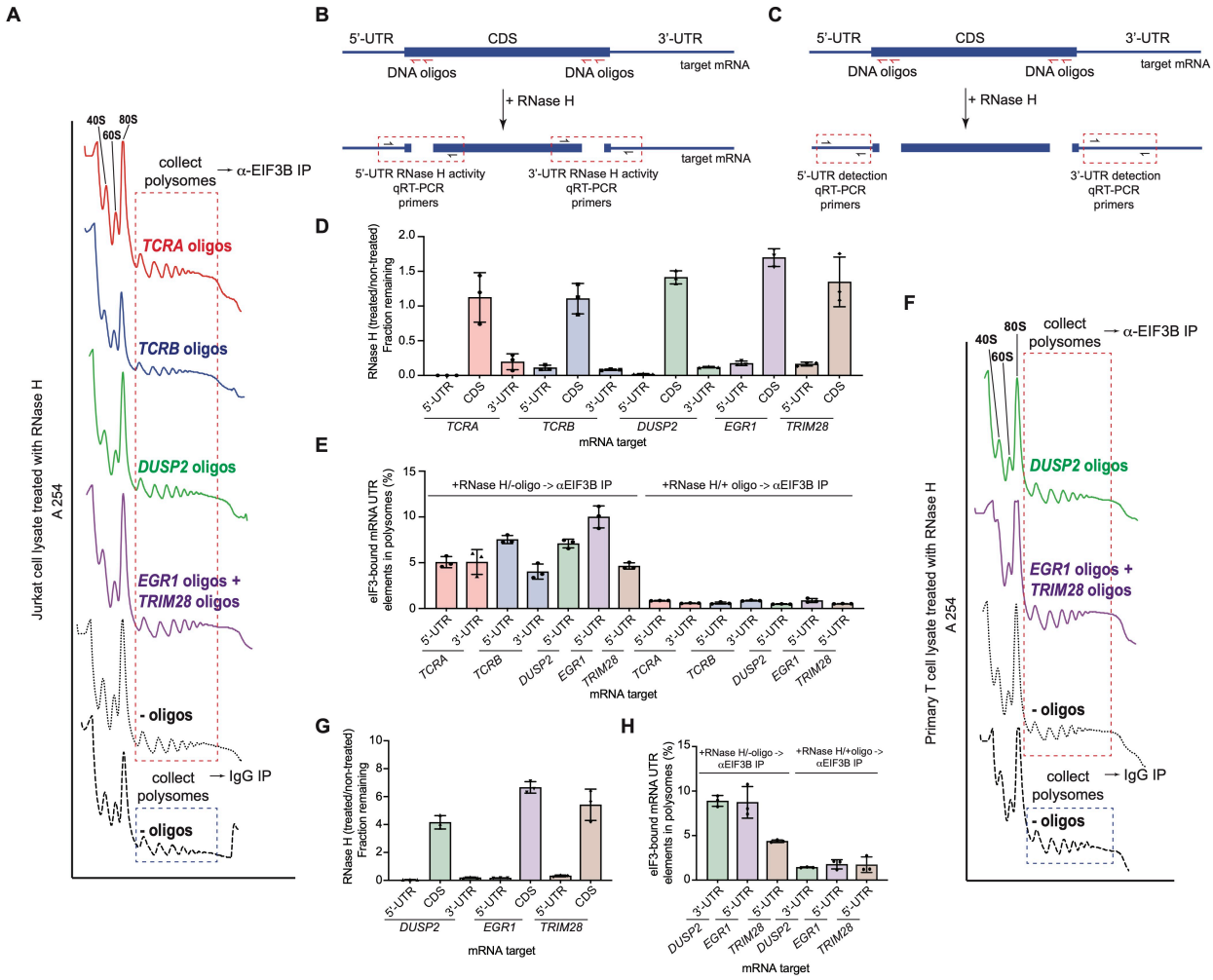

Figure 2–figure supplement 1. The *TCRA* and *TCRB* mRNAs remain bound to elongating ribosomes via eIF3 in activated T cells. (**A**) Sucrose gradient fractionation of polysomes from crosslinked Jurkat cells. Cell lysates treated with RNase H, as indicated, were fractionated on 10%-50% sucrose gradients. Shown is the absorbance at 254 nm, for one of two biological replicates. (**B**) Strategy for detecting mRNA cleavage by RNase H digestion. RT-qPCR primers were designed to span the mRNA digestion sites. (**C**) Strategy for detecting 5'-UTR or 3'-UTR mRNA fragments released by RNase H digestion. RT-qPCR primers were designed within the 5'-UTR or 3'-UTR regions. (**D**) Fraction of intact mRNA segments remaining after RNase H

treatment of DSP-crosslinked cell lysates from Jurkat cells, in the presence or absence of mRNA-specific DNA oligos for the indicated mRNAs. The mRNAs were detected using RT-qPCR oligos as illustrated in panel **B**. (**E**) Amount of eIF3-bound 5'-UTR and 3'-UTR regions of the mRNA co-immunoprecipitated by anti-EIF3B antibody, from polysome fractions of lysate from Jurkat cells treated with RNase H, either in the absence (left) or presence (right) of mRNA-targeting DNA oligos. Percentage is relative to the amount of total mRNA present in the polysome fraction prior to immunoprecipitation. Primers to the mRNA 5'-UTR and 3'-UTR regions, as indicated in panel **C**, were used for quantification**.** (**F**) Sucrose gradient fractionation of polysomes from crosslinked primary human T cells. (**G**) Fraction of intact mRNA segments remaining after RNase H treatment of DSP-crosslinked cell lysates from primary T cells, in the presence or absence of mRNA-specific DNA oligos for the indicated mRNAs. The mRNAs were detected using RT-qPCR oligos as illustrated in panel **B**. (**H**) Amount of eIF3-bound 5'-UTR and 3'-UTR regions of the mRNA co-immunoprecipitated by anti-EIF3B antibody, from polysome fractions of lysate from primary human T cells treated with RNase H, either in the absence (left) or presence (right) of mRNA-targeting DNA oligos. Percentage is relative to mRNA present in the polysome fraction prior to immunoprecipitation. Primers to the mRNA 5'-UTR and 3'-UTR regions, as indicated in panel **C**, were used for quantification. All experiments were carried out in biological duplicate with one technical triplicate shown (n = 3, with mean and standard deviations shown). All the primary human T cell experiments were performed using samples from two donors and data from one representative donor are shown.

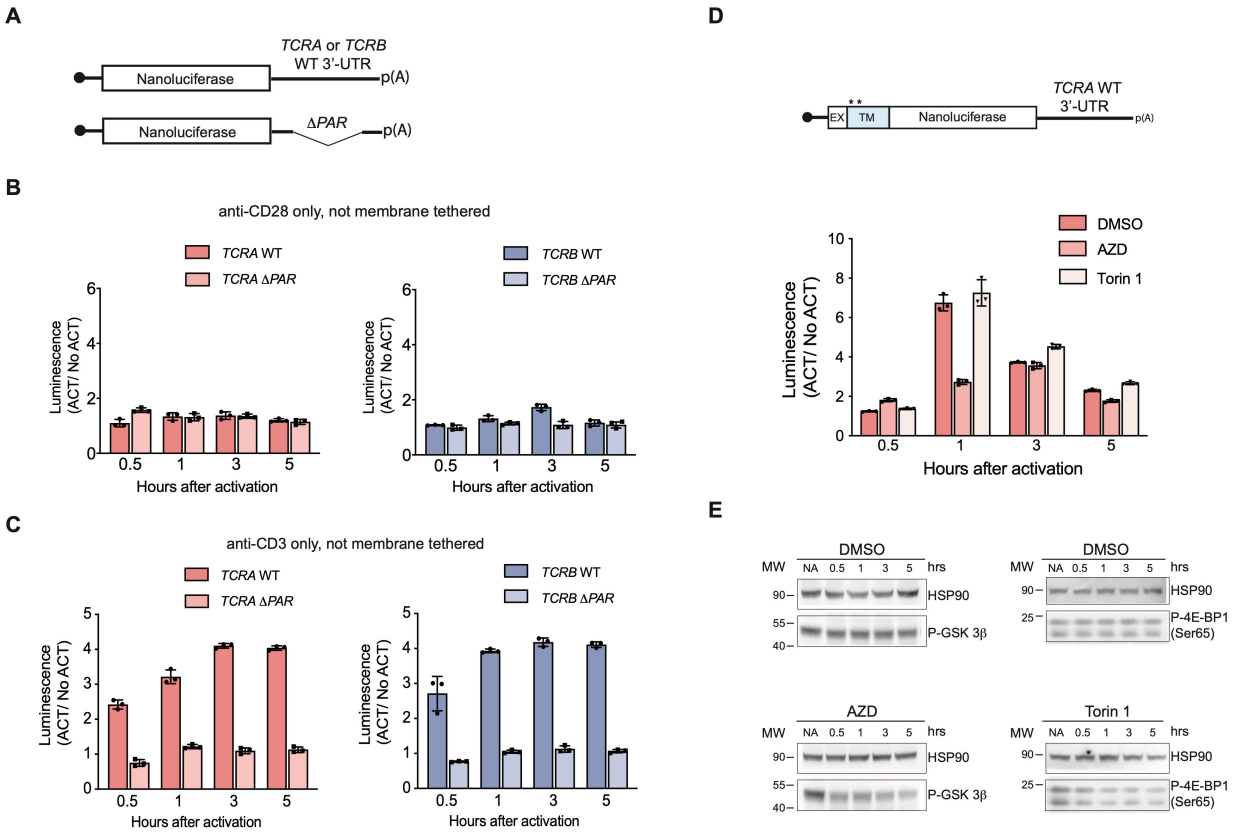

Figure 4–figure supplement 1. Nanoluciferase reporter expression in activated T cells. (**A**) Schematic of nanoluciferase reporters without a transmembrane helix (not membrane tethered) stably expressed in primary human T cells. The reporters carry the *HBB* 5'-UTR and *TCRA, TCRB, TCRA* Δ*PAR,* or *TCRB* Δ*PAR* 3'-UTR. (**B**) Luciferase activity in T cells stably expressing reporters described in **A** stimulated only with anti-CD28 antibodies, relative to non-activated controls (*n* = 3, with mean and standard deviations shown). (**C**) Luciferase activity in primary human T cells stably expressing reporters described in **A** stimulated only with anti-CD3 antibodies, relative to non-activated controls (*n* = 3, with mean and standard deviations shown). (**D**) Luciferase activity in primary human T cells stably expressing membrane-tethered reporter (described in the schematic above) with WT *TCRA* 3'-UTR inhibited with either

AZD5363(AZD) to inhibit AKT activity or Torin 1 to inhibit mTOR before activating with anti-CD3/anti-CD28 antibodies, relative to non-activated controls. In panels **B**–**D**, all experiments were carried out in triplicate (3 separate wells per condition), with mean and standard deviations shown. (**E**) Western blot carried out to measure AKT activity in the presence of AZD5363 (AZD) using an anti-Phospho-GSK-3β antibody or mTOR activity in the presence of Torin 1 using an anti-Phospho-4EBP1 antibody for the samples in **D**. HSP90 was used as a loading control. All the primary human T cell experiments were performed using samples from two donors and data from one representative donor are shown here. The data from the other donor are presented in **Figure 4F**.

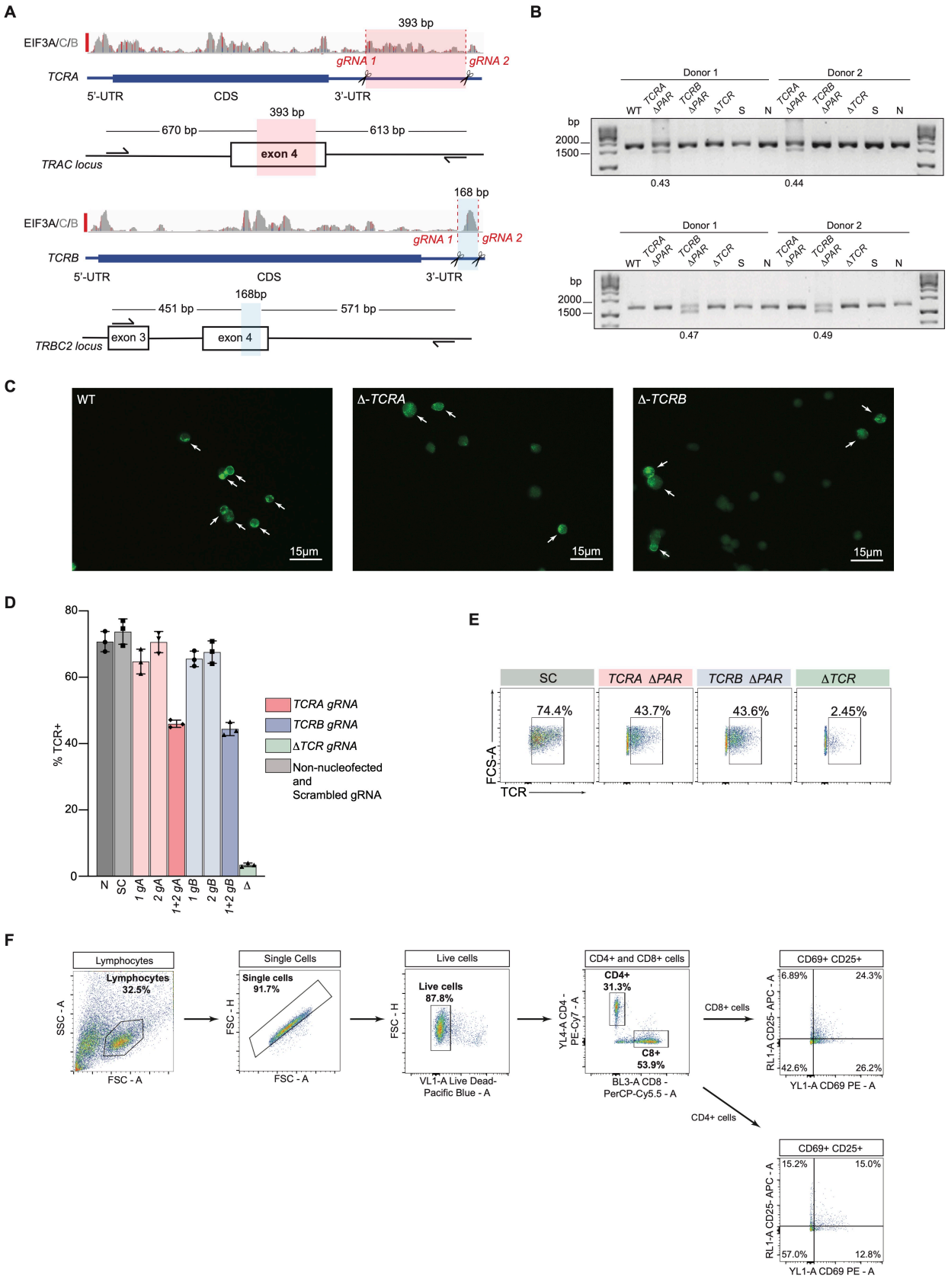

628

Figure 5–figure supplement 1. Generation and analysis of *TCRA* Δ*PAR* and *TCRB* Δ*PAR* primary human T cells. (**A**) CRISPR/Cas9 RNP mediated genome editing at the *TCRA* and *TCRB* genomic loci in primary human T cells. Location of gRNA sites targeting the *TCRA* 3'-UTR, to generate *TCRA* Δ*PAR* cells is highlighted in red. In *TCRA*, gRNA1 and gRNA2 target hg38 genomic locations chr14:22,551,700 and chr14:22,552,073, respectively. Location of gRNA sites targeting the *TCRB* 3'-UTR, to generate *TCRB* Δ*PAR* cells is highlighted in blue. In *TCRB*, gRNA1 and gRNA2 target hg38 genomic locations chr7:142,802,561 and chr7:142,802,695, respectively. (**B**) Top gel: Analysis of *TCRA* 3'-UTR PAR-CLIP site deletion efficiency. Total genomic DNA extracted from WT, *TCRA* Δ*PAR, TCRB* Δ*PAR* (here serving as a negative control), scrambled gRNA nucleofected (S) and non-nucleofected (N) cells was analyzed by PCR to measure the editing efficiency. *TCRA* Δ*PAR* cells produced a 1283 bp PCR product compared to 1676 bp in S, N or *TCRB* Δ*PAR* cells (See panel **A**). Bottom gel: Analysis of *TCRB* 3'-UTR PAR-CLIP site deletion efficiency. Total genomic DNA extracted from WT, *TCRA* Δ*PAR* (here serving as a negative control)*, TCRB* Δ*PAR*, scrambled gRNA nucleofected (S) and non-nucleofected (N) cells were analyzed by PCR to measure the editing efficiency. *TCRB* Δ*PAR* cells produced a 1022 bp PCR product compared to 1190 bp in S, N or *TCRA* Δ*PAR* cells (See panel **A**). The percentage of alleles with PAR-CLIP site deletion, quantified by imageJ. (**C**) Representative immunofluorescence images used to count TCR clusters in WT, *TCRA* Δ*PAR* and *TCRB* Δ*PAR* primary human T cells. The white arrows indicate the cells that were scored as having TCR clusters. (**D**) Percentage of cells expressing TCR on the cell surface of activated T cells measured by flow cytometric analysis. TCR expressing cells in the cell populations tested: *N*, Non-nucleofected cells;

SC, Scrambled gRNA; *1gA*, *TCRA* gRNA 1; *2gA*, *TCRA* gRNA 2; *1+2 gA*, *TCRA* gRNA 1+2 (i.e. *TCRA* Δ*PAR*); *1gB*, *TCRB* gRNA 1; *2gB*, *TCRB* gRNA 2; *1+2 gB*, *TCRB* gRNA 1+2 (i.e. *TCRB* Δ*PAR*); Δ*TCR*, TCR gRNA targeting the CDS of *TCRA*. (*n* = 3 replicates from three separate wells, with mean and standard deviation shown.) (**E**) Representative density plots showing the percentage of TCR on the cell surface in activated T cells. The cell lines shown are: SC, *TCRA* Δ*PAR*, *TCRB* Δ*PAR*, Δ*TCR* (negative control). In panels **D** and **E**, representative results from one of two donors are shown. (**F**) Gating strategy for flow cytometric analysis of CD69 and CD25 levels. Primary human T cells were gated to isolate lymphocytes, followed by isolation of single cells, then live cells. Next, cells were gated to separate CD4+ and CD8+ cells expressing T cell activation markers CD69 and CD25. Shown is the workflow of the FACS gating, with an example of T cells activated with anti-CD3/anti-CD28 antibodies for 8 hours.

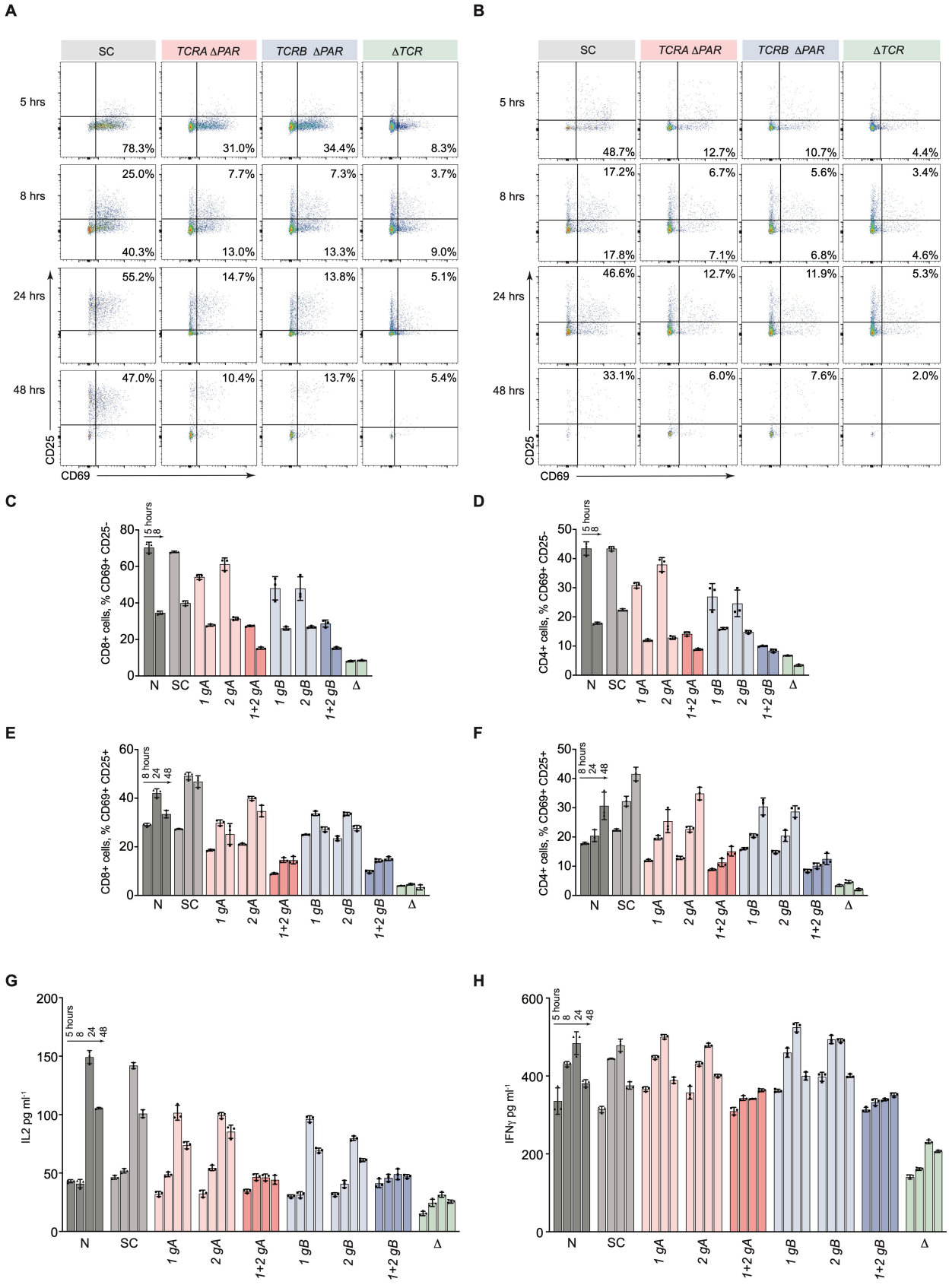

667

Figure 5–figure supplement 2. Effects of *TCRA* Δ*PAR* and *TCRB* Δ*PAR* mutations on different steps of T cell activation. (A and **B)** Representative density plots showing the percentage of, **A** CD8+ T cells and **B**, CD4+ T cells expressing CD69 (early activation marker), CD25 (mid-activation marker) or CD69 and CD25 after activation with anti-CD3/anti-CD28 antibodies at different time points, analyzed by flow cytometry. The plots represent one of the two donors. The cell lines shown are SC, *TCRA* Δ*PAR*, *TCRB* Δ*PAR* and Δ*TCR* (negative control). **(C** and **D)** Flow cytometric analysis quantifying the mean percent of **C,** CD8+ T and **D**, CD4+ T cells that are only CD69+. **(E** and **F)** Flow cytometric analysis quantifying the mean percent of **E,** CD8+ T and **F**, CD4+ T cells that are CD69+CD25+. (**G** and **H**) Quantification of **G**, secreted IL-2 and **H**, secreted IFNγ, for all cell populations tested, as determined by ELISA. In panels **C**–**H** cell populations tested: N, Non-nucleofected cells; SC, Scrambled gRNA; *1gA*, *TCRA* gRNA 1; *2gA*, *TCRA* gRNA 2; *1+2 gA*, *TCRA* gRNA 1+2 (i.e. *TCRA* Δ*PAR*); *1gB*, *TCRB* gRNA 1; *2gB*, *TCRB* gRNA 2; *1+2 gB*, *TCRB* gRNA 1+2 (i.e. *TCRB* Δ*PAR*); *ΔTCR* gRNA targeting the CDS of *TCRA*. In panels **C** through **H**, all experiments were carried out in triplicate (3 separate wells per condition), with mean and standard deviations shown. Representative results from one donor are shown.

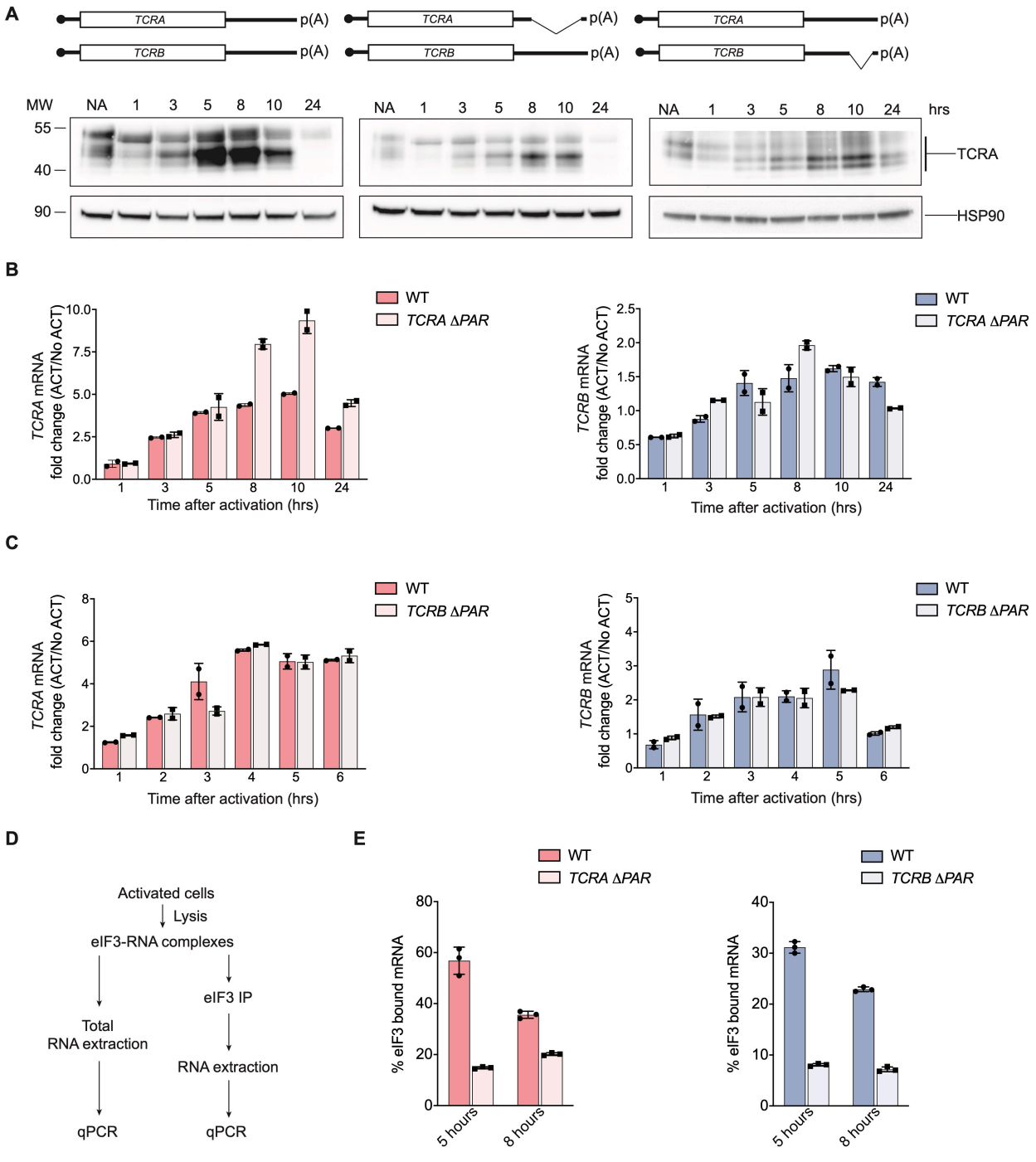

688

689 **Figure 5–figure supplement 3. eIF3 binding to the *TCRA* and *TCRB* mRNA 3'-UTR**

690 **elements in Jurkat cells.** (**A**) Western blots of TCRA protein levels as a function of time

691 after anti-CD3/anti-CD28 activation. Cell lines used: WT Jurkat cells, *TCRA* Δ*PAR* and

692 *TCRB* Δ*PAR*, Jurkat cells in which the eIF3 PAR-CLIP sites in the 3'-UTRs of the *TCRA*

and *TCRB* mRNAs, respectively, have been deleted. Schematics of *TCRA* and *TCRB* mRNAs with and without eIF3 PAR-CLIP sites are shown above. HSP90 was used as a loading control. Western blots are representative of two biological replicates. (**B**) *TCRA* and *TCRB* mRNA levels in WT Jurkat cells, or Jurkat cells with the *TCRA* eIF3 3'-UTR PAR-CLIP site deleted, as determined by qRT-PCR at different time points after anti-CD3/anti-CD28 activation. (**C**) *TCRA* and *TCRB* mRNA levels in WT Jurkat cells, or Jurkat cells with the *TCRB* eIF3 3'-UTR PAR-CLIP site deleted, as determined by qRT-PCR at different time points after anti-CD3/anti-CD28 activation. (**D**) Schematic of immunoprecipitation of eIF3 using an anti-EIF3B antibody, followed by qRT-PCR to quantify the amount of nanoluciferase mRNA bound to eIF3. (**E**) Immunoprecipitation of eIF3 as shown in **D** to quantify the amount of *TCRA* or *TCRB* mRNA bound to eIF3 in Jurkat cells after activation with anti-CD3/anti-CD28 antibodies for 5 hours (left) and 8 hours (right). The percent mRNA bound to anti-EIF3B beads is calculated relative to total mRNA isolated from the cells. In panels **B**–**E**, all experiments were carried out in triplicate (3 separate wells per condition), with mean and standard deviations shown. Representative results from one of two biological replicates are shown.

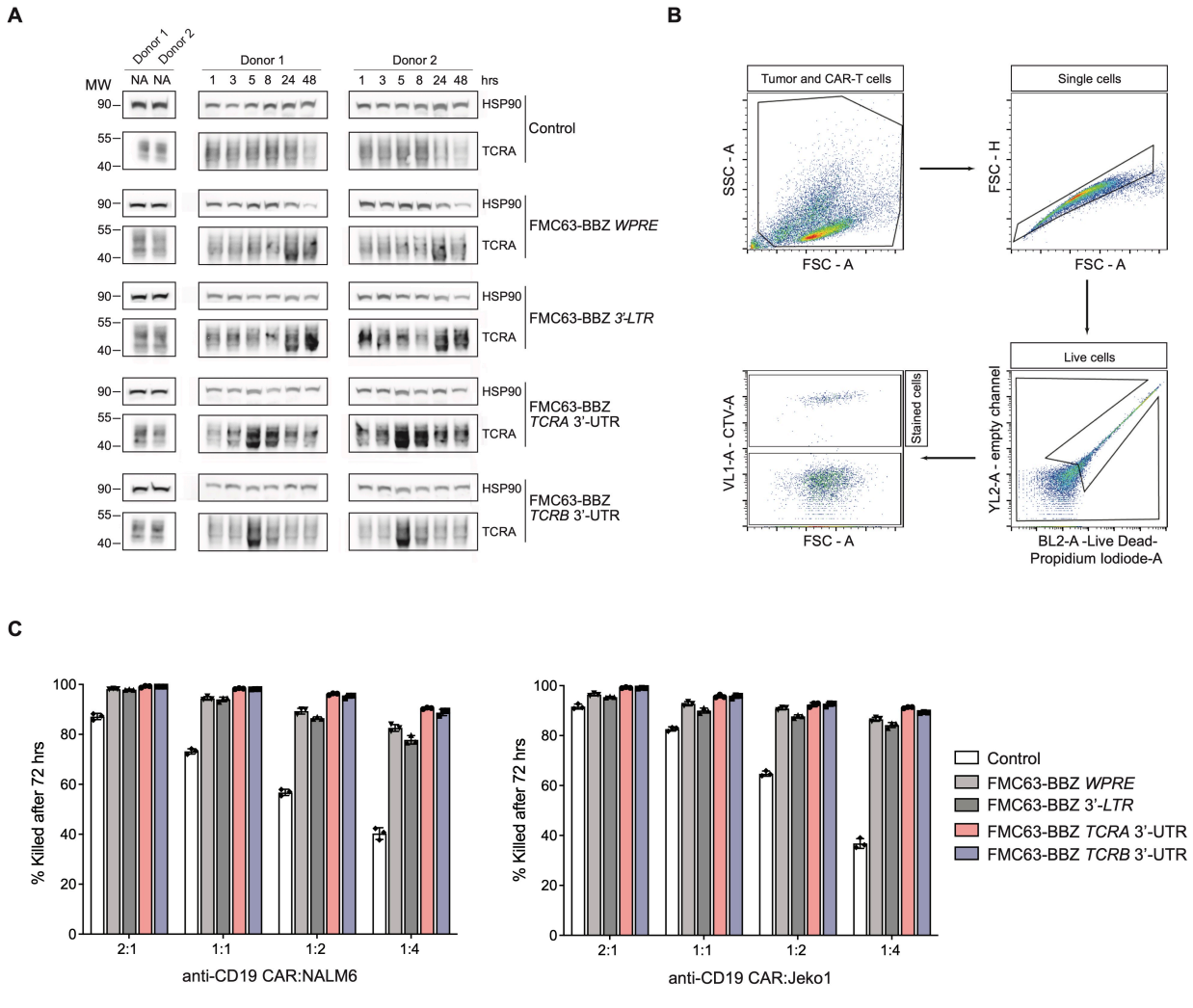

Figure 6–figure supplement 1. Effects of the *TCRA* and *TCRB* mRNA 3'-UTR elements on CAR T cell function. (**A**) Western blots measuring TCRA protein levels as a function of time in FMC63-BBZ CAR T cells after incubation with NALM6 tumor cells. Cell lines used are labeled: Control, *WPRE, 3'-LTR, TCRA* and *TCRB* 3'-UTR diagrammed in **Figure 6B**. HSP90 was used as a loading control. (**B**) Gating strategy for flow cytometric analysis to detect live tumor cells after incubation with CAR T cells. This includes: (1) both CAR T and tumor cell gating, (2) isolating single cells, (3) isolating live cells based on propidium iodide staining and (4) separating cell trace violet (CTV) stained vs non-stained cells to isolate live tumor cells. (**C**) Cytotoxic activity of FMC63-BBZ CARs

721 fused to various 3'-UTRs described in **Figure 6B** after incubating with NALM6 or Jeko1
722 tumor cell lines for 72 hours. Representative results for one of two donors are shown (*n*
723 = 3 separate wells, with mean and standard deviations shown).

724

725

726

727

Supplementary Files

Supplementary File 1. (Separate file) Subunits in eIF3 crosslinked to RNA in activated Jurkat cells. Lists the eIF3 subunits, percent sequence coverage and number of identified peptides.

Supplementary File 2. (Separate file) PARpipe statistics for eIF3 PAR-CLIP samples. Samples are indexed in the first tab, including both biological replicates for activated and non-activated Jurkat cells. Statistics are given for each library at the read, cluster and group level.

Supplementary File 3. (Separate file) PAR-CLIP mapping to individual genes for each eIF3 PAR-CLIP sample. Samples are indexed in the first tab, including both biological replicates for activated and non-activated Jurkat cells. First lists the gene name and number of clusters identified. The statistics also include: Sum, sum of that statistic over all sites for that gene; Med, median of that statistic for all sites for that gene; ReadCount, total reads mapping to the gene; T2C fraction, number of reads with T-to-C conversions / number of reads; ConversionSpecificity, log (number of reads with T-to-C conversions / number of reads with other conversions); UniqueReads, reads collapsed to single copies. Also included: 5'utr/Intron/Exon/3'utr/Start_codon/Stop_codon, number of sites mapping to that annotation category; Junction, number of sites mapping to a junction

749 between categories (coding-intron, coding-3'utr, etc.); GeneType, as described in the
750 gene_type category for this gene in the .gtf file used.

751

752 **Supplementary File 4. (Separate file) Transcriptome analysis of non-activated or**
753 **activated Jurkat cells.** Each tab lists transcript name and version, gene name, type of
754 transcript, length of transcript, and mean transcripts per million, calculated from two
755 biological replicates.

756

757 **Supplementary File 5. (Separate file) Pathway enrichment analysis.** Lists for both
758 biological replicates of the EIF3A/C/B PAR-CLIP libraries are included (genes with >= 100
759 reads), along with associated transcript names, lengths in nts of the 5'-UTR, coding
760 region, and 3'-UTR, and reads normalized to the lengths of the transcript regions. Tabs
761 also include the top tissue-specific pathway enrichment categories determined using the
762 STRING Database. These list: the Gene Ontology (GO) number, GO description,
763 observed gene count, background gene count, false discovery rate, and matching
764 proteins in the network by Ensembl protein ID, and by gene name.

765

766 **Supplementary File 6. (Separate file) Reagent information for experiments.** Lists
767 include antibodies used, PCR primers, qPCR primers, gRNA targeting sequences, and
768 FISH probes, and DNA oligos for RNase H experiments.

769

770

References

Ascano, M., Hafner, M., Cekan, P., Gerstberger, S., and Tuschl, T. (2012). Identification of RNA-protein interaction networks using PAR-CLIP. Wiley Interdiscip. Rev. RNA *3*, 159–177.

Bray, N.L., Pimentel, H., Melsted, P., and Pachter, L. (2016). Near-optimal probabilistic RNA-seq quantification. Nat. Biotechnol. *34*, 525–527.

Call, M.E., Pyrdol, J., Wiedmann, M., and Wucherpfennig, K.W. (2002). The organizing principle in the formation of the T cell receptor-CD3 complex. Cell.

Corcoran, D.L., Georgiev, S., Mukherjee, N., Gottwein, E., Skalsky, R.L., Keene, J.D., and Ohler, U. (2011). PARalyzer: definition of RNA binding sites from PAR-CLIP short-read sequence data. Genome Biol. *12*, R79.

Cunningham, F., Achuthan, P., Akanni, W., Allen, J., Amode, M.R., Armean, I.M., Bennett, R., Bhai, J., Billis, K., Boddu, S., et al. (2019). Ensembl 2019. Nucleic Acids Res. *47*, D745–D751.

Danan, C., Manickavel, S., and Hafner, M. (2016). PAR-CLIP: A Method for Transcriptome-Wide Identification of RNA Binding Protein Interaction Sites. Methods Mol. Biol. *1358*, 153–173.

Dong, D., Zheng, L., Lin, J., Zhang, B., Zhu, Y., Li, N., Xie, S., Wang, Y., Gao, N., and Huang, Z. (2019). Structural basis of assembly of the human T cell receptor-CD3 complex. Nature *573*, 546–552.

Frankish, A., Diekhans, M., Ferreira, A.-M., Johnson, R., Jungreis, I., Loveland, J., Mudge, J.M., Sisu, C., Wright, J., Armstrong, J., et al. (2019). GENCODE reference annotation for the human and mouse genomes. Nucleic Acids Res. *47*, D766–D773.

Hall, M.P., Unch, J., Binkowski, B.F., Valley, M.P., Butler, B.L., Wood, M.G., Otto, P., Zimmerman, K., Vidugiris, G., Machleidt, T., et al. (2012). Engineered luciferase reporter from a deep sea shrimp utilizing a novel imidazopyrazinone substrate. ACS Chem. Biol. *7*, 1848–1857.

June, C.H., Levine, B.L., Porter, D.L., Kalos, M.D., and Milone, M.C. (2014). Compositions for treatment of cancer.

Kalos, M., Levine, B.L., Porter, D.L., Katz, S., Grupp, S.A., Bagg, A., and June, C.H. (2011). T cells with chimeric antigen receptors have potent antitumor effects and can establish memory in patients with advanced leukemia. Sci. Transl. Med. *3*, 95ra73.

Kochenderfer, J.N., Feldman, S.A., Zhao, Y., Xu, H., Black, M.A., Morgan, R.A., Wilson, W.H., and Rosenberg, S.A. (2009). Construction and preclinical evaluation of an anti-CD19 chimeric antigen receptor. J. Immunother. *32*, 689–702.

Lee, A.S.Y., Kranzusch, P.J., and Cate, J.H.D. (2015). eIF3 targets cell-proliferation messenger RNAs for translational activation or repression. Nature *522*, 111–114.

Martin, M. (2011). Cutadapt removes adapter sequences from high-throughput sequencing reads. EMBnet.journal *17*, 10–12.

Milone, M.C., Fish, J.D., Carpenito, C., Carroll, R.G., Binder, G.K., Teachey, D.,

Samanta, M., Lakhal, M., Gloss, B., Danet-Desnoyers, G., et al. (2009). Chimeric receptors containing CD137 signal transduction domains mediate enhanced survival of T cells and increased antileukemic efficacy in vivo. Mol. Ther. *17*, 1453–1464.

Mukherjee, N., Wessels, H.-H., Lebedeva, S., Sajek, M., Ghanbari, M., Garzia, A., Munteanu, A., Yusuf, D., Farazi, T., Hoell, J.I., et al. (2019). Deciphering human ribonucleoprotein regulatory networks. Nucleic Acids Res. *47*, 570–581.

Noguchi, S., Arakawa, T., Fukuda, S., Furuno, M., Hasegawa, A., Hori, F., Ishikawa-Kato, S., Kaida, K., Kaiho, A., Kanamori-Katayama, M., et al. (2017). FANTOM5 CAGE profiles of human and mouse samples. Sci Data *4*, 170112.

Parslow, A., Cardona, A., and Bryson-Richardson, R.J. (2014). Sample drift correction following 4D confocal time-lapse imaging. J. Vis. Exp.

Roth, T.L., Puig-Saus, C., Yu, R., Shifrut, E., Carnevale, J., Li, P.J., Hiatt, J., Saco, J., Krystofinski, P., Li, H., et al. (2018). Reprogramming human T cell function and specificity with non-viral genome targeting. Nature *559*, 405–409.

Schumann, K., Lin, S., Boyer, E., Simeonov, D.R., Subramaniam, M., Gate, R.E., Haliburton, G.E., Ye, C.J., Bluestone, J.A., Doudna, J.A., et al. (2015). Generation of knock-in primary human T cells using Cas9 ribonucleoproteins. Proc. Natl. Acad. Sci. U. S. A. *112*, 10437–10442.

Szklarczyk, D., Gable, A.L., Lyon, D., Junge, A., Wyder, S., Huerta-Cepas, J., Simonovic, M., Doncheva, N.T., Morris, J.H., Bork, P., et al. (2019). STRING v11: protein-protein association networks with increased coverage, supporting functional

discovery in genome-wide experimental datasets. Nucleic Acids Res. *47*, D607–D613.

Voon, D.C., Subrata, L.S., Baltic, S., Leu, M.P., Whiteway, J.M., Wong, A., Knight, S.A., Christiansen, F.T., and Daly, J.M. (2005). Use of mRNA- and protein-destabilizing elements to develop a highly responsive reporter system. Nucleic Acids Res. *33*, e27.

Wickham, H., Chang, W., and Others (2016). ggplot2: Create elegant data visualisations using the grammar of graphics. R Package Version *2*.